Journal of Chromatography, 548 (1991) 25–60
Elsevier Science Publishers B.V., Amsterdam

CHROMSYMP. 2206

Evaluation of kinetic models for biospecific adsorption and its implications for finite bath and column performance

M. A. McCOY and A. I. LIAPIS*
Department of Chemical Engineering and Biochemical Processing Institute, University of Missouri-Rolla, Rolla, MO 65401-0249 (USA)

ABSTRACT

Dynamic models that could describe the adsorption of adsorbate onto ligand immobilized on porous or non-porous particles in batch and column systems, are presented and solved.

Two different kinetic models (kinetic models 1 and 2) are used to describe the dynamics of the adsorption mechanism when β-galactosidase is adsorbed onto monoclonal antibody immobilized on porous silica particles. The differences in the theoretical predictions of the concentration of the adsorbate in the fluid of the finite bath obtained from kinetic models 1 and 2, are not significant and the agreement between experiment and theory is good. But the two different kinetic models lead to different estimates for the value of the pore diffusivity, and provide significantly different concentration profiles for the adsorbate in the pore fluid and adsorbed phases of the adsorbent particles of the batch system. The column results indicate that the differences in the breakthrough curves obtained from kinetic models 1 and 2, increase as the column length increases. Also, the concentration profiles of the adsorbate in the adsorbent particles obtained from kinetic models 1 and 2, are significantly different and their differences vary along the axial distance of the column. The results indicate that while it is a necessary condition for a kinetic model to describe properly the experimental overall mass-transfer resistance, this is not also a sufficient condition for the accurate determination of the adsorption mechanism and for the accurate estimation of the values of the rate constants and of the pore diffusivity. Furthermore, the differences in the concentration profiles of the adsorbate in the adsorbent particles, obtained from kinetic models 1 and 2, have important implications on the performance of the adsorption stage, as well as on the performance of the wash and elution stages. Experiments are suggested which could provide information that could significantly improve the model discrimination and parameter estimation studies for the determination of a proper mechanism for the dynamics of the adsorption step and of an accurate estimate for the value of the pore diffusivity. When the estimated value of the pore diffusivity is varied by $\pm 20\%$, the effect on the dynamic behavior of the batch and column systems can be appreciable. The effect on the dynamic behavior of the batch and column systems when the estimated value (from a correlation) of the film mass transfer coefficient is varied by $\pm 20\%$, is not significant.

The batch adsorption of β-galactosidase onto anti-β-galactosidase immobilized on non-porous glass coated beads is found to be controlled by film mass transfer and the dynamics of the adsorption step. The batch model with a second-order reversible interaction mechanism for the adsorption step, provides theoretical predictions such that the agreement between experiment and theory is reasonable. When the estimated value (from a correlation) of the film mass transfer coefficient is varied by $\pm 20\%$, the effect on the dynamic behavior of the batch and column systems (having nonporous adsorbent particles) is not significant. Column experiments are suggested which could provide information, in addition to the information obtained from batch experiments, that could improve the model discrimination and parameter estimation studies for the determination of a proper mechanism for the dynamics of the adsorption step, in affinity adsorption systems involving non-porous adsorbent particles.

0021-9673/91/$03.50

INTRODUCTION

Industry has significant interest in the design, optimization, and control of large-scale affinity adsorption systems which are to be employed in the purification of biologically active macromolecules for use as pharmaceuticals or in other applications where the purity of the product is a very important consideration. Certain fundamental mechanisms underlying the affinity adsorption separations have been identified and constitutive expressions which may be used to quantify these mechanisms and their effects, have been suggested and constructed [1–19]. The parameters characterizing the mechanisms involved in the different stages (*i.e.*, adsorption, wash, elution) of affinity adsorption and in the different operational modes [*i.e.*, batch, fixed bed (column), fluidized bed] could be estimated from proper correlations and/or by matching the predictions of appropriate models, which are developed to describe the behavior of affinity adsorption in the different stages and operational modes, with experimental data [1–4,11–20].

It is well established that affinity adsorption experiments are tedious, time consuming, and expensive. The number of experiments at the bench-scale and pilot-scale levels could be significantly reduced by developing and employing mathematical models that would satisfactorily predict the behavior of the affinity adsorption stages under different operational modes. Such models may be used to guide the experiments [1,11–14,16,18–21] in regions of the experimental space where a better scientific understanding of the behavior of affinity adsorption mechanisms may be obtained, and even new and interesting phenomena might be observed. Furthermore, these models could be used in the complex tasks of design, optimization, control, and scale-up of affinity adsorption processes. It should be emphasized that there is nothing more practical than a mathematical model which can accurately predict the dynamic behavior, scale-up, and design of a process of interest, since such a model could obviate many experiments which in the case of affinity chromatography are tedious, time consuming, and expensive.

In this work, the dynamic behavior of the adsorption of β-galactosidase onto monoclonal antibody ligand immobilized on (a) porous silica particles and on (b) non-porous glass coated beads, is studied by two different kinetic models that characterize the dynamics of the interaction (adsorption step) between the adsorbate and ligand. Also, the effects on the dynamic behavior of biospecific adsorption of the parameters that characterize film mass transfer and intraparticle diffusion, are examined. Both finite bath (batch) and column (fixed bed) adsorption systems are considered.

THEORY

Single component adsorption is considered to occur, and the mass transfer and interaction steps are as follows: (i) The transport of adsorbate from the bulk fluid to the external surface of the adsorbent particle (film mass transfer). (ii) The transport of adsorbate within the porous adsorbent particle (intraparticle diffusion); in case that the adsorbent particle is non-porous, intraparticle diffusion does not occur. (iii) The interaction between the adsorbate and the immobilized ligand (adsorption step). The interaction step (iii) may be composed of several substeps, depending on the

complexity of the adsorbate–ligand interaction, and could include the binding of multivalent adsorbates to monovalent ligands [1,4,11]. Yon [11] has shown that in most affinity chromatography systems the partitioning will seem to be monovalent, *i.e.*, interaction between a monovalent adsorbate and a monovalent ligand. In this work, the partitioning is considered as being monovalent.

The most commonly used mode of operation in affinity chromatography separations is the fixed bed mode with axial flow [2,4,10,14,16]. Batch (finite bath) adsorption systems would be appropriate where the fluid to be processed was of high viscosity or contains particulate material. Arve and Liapis [1], Liapis [14–17] and Petropoulos *et al.* [12] have indicated that, for a given affinity adsorption system, the parameters that characterize the intraparticle mass transfer and adsorption mechanisms should be independent of the operational mode (*e.g.*, batch, fixed bed, fluidized bed), and therefore, if these parameters are estimated by utilizing information obtained from finite bath experiments (batch experiments are easier to perform and analyze [1,10,14–20] than column experiments), then their values should characterize the intrinsic mechanisms (intraparticle mass transfer and adsorption mechanisms) in other operational modes. This theoretical approach of Arve and Liapis [1] has been shown to be valid by the data of the affinity chromatography system studied by Horstmann and Chase [22]. Furthermore, Johnston and Hearn [20] compared the experimental dynamic adsorption data of the binding of several proteins (with different molecular geometries) to several ion-exchange and dye-affinity chromatographic resins, with the theoretical predictions of different models. They found [20] that the model of Arve and Liapis [1,4] provided the best agreement between experiment and theory, and furthermore, the values of the kinetic parameters estimated by matching the theoretical predictions of this model with the experimental data, were found [20] to be consistent with enzyme kinetic theory.

Finite bath with porous adsorbent particles

The porous adsorbent particles are suspended in the liquid of the finite bath by agitation so that the liquid has free access, and the bulk concentration of the adsorbate is taken to be uniform throughout the bath except in a thin film (film mass transfer resistance) of liquid surrounding each particle. The adsorption process is considered to be isothermal since the heat of adsorption apparently does not change the temperature [13,14–16,19] of the liquid phase even in large-scale systems; this occurs because the total amount of adsorbed material is small and the heat capacity of the liquid phase is high.

A differential mass balance for the adsorbate in the fluid phase of the finite bath gives

$$\frac{dC_d}{dt} = \left(\frac{1-\varepsilon}{\varepsilon}\right)\left(\frac{\alpha+1}{r_0}\right) K_f[C_p(t,r_0) - C_d] \tag{1}$$

Eqn. 1 can be used for particles having geometry of slab, cylinder or sphere by putting $\alpha = 0$, 1 or 2, respectively. The initial condition of eqn. 1 is given by

$$C_d = C_{d0} \qquad \text{at} \qquad t = 0 \tag{2}$$

The transport of the adsorbate in the adsorbent particle is considered to be governed by the diffusion [1,12] of the species in the pore fluid (pore diffusion) of the particle. The intraparticle (pore diffusion) transport mechanism is taken to be one-dimensional and in particles that have an axis of symmetry. It is understood that in the case of the slab and the cylinder, the particles are of infinite extent or alternatively one must artificially assume that the ends of a finite cylinder or edges of a finite slab are sealed in order to keep the problem one-dimensional. A differential material balance for the adsorbate in the adsorbent particle is given by

$$\frac{\partial(\varepsilon_p C_p)}{\partial t} + \frac{\partial C_s}{\partial t} = \frac{1}{r^\alpha}\frac{\partial}{\partial r}\left(r^\alpha \varepsilon_p D_p \frac{\partial C_p}{\partial r}\right) \tag{3}$$

The initial and boundary conditions for eqn. 3 are

$$C_p = 0 \qquad \text{at} \qquad t = 0, \qquad 0 \leqslant r \leqslant r_0 \tag{4}$$

$$C_s = 0 \qquad \text{at} \qquad t = 0, \qquad 0 \leqslant r \leqslant r_0 \tag{5}$$

$$\varepsilon_p D_p \left.\frac{\partial C_p}{\partial r}\right|_{r=r_0} = K_f[C_d - C_p(t,r_0)], \qquad t > 0 \tag{6}$$

$$\left.\frac{\partial C_p}{\partial r}\right|_{r=0} = 0, \qquad t > 0 \tag{7}$$

If restricted [12,20] pore diffusion occurs, then ε_p and D_p would vary with the loading of the adsorbate in the adsorbed phase, as shown by the restricted pore diffusion mathematical model of Petropoulos *et al.* [12]. If the effect of restricted pore diffusion on the mass flux of the adsorbate is not significant, then the values of ε_p and D_p may be considered to be constant [1,12,20].

It is apparent that eqn. 3 can be solved only if an appropriate expression for the term $\partial C_s/\partial t$ is available. This term represents the accumulation of the adsorbed species on the internal surface of the porous adsorbent particle, and it can be quantified if a mathematical expression could be constructed that would describe the mechanism of the adsorption of the adsorbate onto the immobilized ligand. In this work, two different kinetic models for the adsorption mechanism are considered:

(1) The adsorption is completely reversible and with no interaction between the adsorbed molecules. The interaction between unbound monovalent adsorbate (A_1) in the solution and vacant immobilized monovalent ligand (L_1) may be considered to be of the form [1,5,6,13,14,20,22]

$$A_1 + L_1 \underset{k_{21}}{\overset{k_{11}}{\rightleftarrows}} A_1L_1 \tag{8}$$

where A_1L_1 represents the non-covalent adsorbate–ligand complex. Then assuming elementary interactions, the rate of the adsorption step may be described by the following second-order reversible interaction:

$$\frac{\partial C_s}{\partial t} = k_{11}C_p(C_T - C_s) - k_{21}C_s \tag{9}$$

The subscript 1 in the rate constants k_{i1} ($i = 1, 2$), indicates that these parameters characterize the forward and reverse rates of the second-order interaction given by kinetic model 1. This model is described by eqn. 8 and its dynamic expression is given by eqn. 9. The accumulation term, $\partial C_s/\partial t$, in eqn. 9 becomes equal to zero when adsorption equilibrium is established, and the following expression for the equilibrium isotherm is obtained:

$$C_s = \frac{C_T K C_p}{1 + K C_p} \tag{10}$$

Eqn. 10 represents the Langmuir equilibrium adsorption model where $K = k_{11}/k_{21}$. It should be noted that at equilibrium the value of C_p in eqn. 10 should be equal to the value of C_d.

The initial condition of eqn. 9 is given by eqn. 5. Eqns 1, 3 and 9 could now be solved simultaneously in order to obtain the dynamic behavior of C_d, C_p and C_s. It should be noted at this point that if the interaction between the adsorbate and ligand occurs infinitely fast, then the adsorbate molecules in the solution and in the adsorbed phase are in equilibrium at every point in the pore and the term $\partial C_s/\partial t$ in eqn. 3 would take the following form (eqn. 10 is employed):

$$\frac{\partial C_s}{\partial t} = \left(\frac{\partial C_s}{\partial C_p}\right)\left(\frac{\partial C_p}{\partial t}\right) = \left[\frac{C_T K}{(1 + K C_p)^2}\right]\left(\frac{\partial C_p}{\partial t}\right) \tag{11}$$

(2) Lundstrom *et al.* [6] have indicated that, in certain systems, macromolecule-induced exchange interactions may occur on the surface of the adsorbent, whereby an already adsorbed molecule is exchanged with a protein molecule from the solution; this process may occur even if the spontaneous desorption of biomolecules is very small. They have suggested a kinetic model for the adsorption step, which may be considered for systems where the volume of the immobilized ligand is smaller than the volume of the adsorbate molecule. It is assumed that a biomolecule adsorbs on the surface forming one type of adsorbate–ligand complex ("form a"), and that after adsorption it may change conformation ("form b"). An adsorbed molecule in "form a" is considered to occupy an area A_a on the surface, while an adsorbed molecule in "form b" is considered to occupy an area A_b. The adsorbed molecules of "form a" and "form b" are competing for the same area on the surface, and it is assumed that both exchange interactions and spontaneous desorption take place on the surface. The exchange interactions are modelled as a desorption, which depends on the concentration of the adsorbate in the pore fluid, $C_p(t,r)$. If C_T now represents the available adsorption sites for molecules of "form a" and δ represents the ratio of A_b to A_a ($\delta = A_b/A_a$), then the interaction rate expressions for this physical model are

$$\frac{\partial C_{sa}}{\partial t} = (k_{12} C_p - k_{32} C_{sa})(C_T - C_{sa} - \delta C_{sb}) - k_{42} C_p C_{sa} - k_{22} C_{sa} \tag{12}$$

$$\frac{\partial C_{sb}}{\partial t} = k_{32} C_{sa}(C_T - C_{sa} - \delta C_{sb}) - k_{62} C_p C_{sb} - k_{52} C_{sb} \tag{13}$$

where C_{sa} and C_{sb} represent the concentrations of the adsorbate in the complexes of "form a" and "form b", respectively. The parameters k_{i2} ($i = 1, 2, \ldots, 6$) are interaction rate constants. The parameters k_{22} and k_{52} characterize the spontaneous desorption of adsorbate from complexes of "form a" and "form b", respectively. The rate constants k_{42} and k_{62} characterize macromolecule-induced exchange interactions from complexes of "form a" and "form b", respectively. The parameter k_{12} characterizes the rate of formation of the complex of "form a" by the forward interaction between adsorbate in the solution (pore fluid) and immobilized vacant ligand. The rate constant k_{32} characterizes the rate of formation of the complex of "form b" from the complex of "form a". The subscript 2 in the rate constants k_{i2} ($i = 1, 2, 3, \ldots, 6$) indicates that these parameters characterize the interactions described by kinetic model 2. This model is described by the dynamic expressions shown in eqns. 12 and 13. The accumulation term, $\partial C_s/\partial t$, in eqn. 3 is obtained from the terms $\partial C_{sa}/\partial t$ and $\partial C_{sb}/\partial t$. It should be noted that the equilibrium expressions for C_{sa} and C_{sb} are obtained from eqns. 12 and 13 by setting the accumulation terms ($\partial C_{sa}/\partial t$, $\partial C_{sb}/\partial t$) equal to zero. Furthermore, at $t = 0$ the concentrations C_{sa} and C_{sb} are considered to be equal to zero, and thus, $C_s = C_{sa} + C_{sb} = 0$ (eqn. 5) at $t = 0$. Eqns. 1, 3 and 12 and 13 could now be solved simultaneously in order to obtain the dynamic behavior of C_d, C_p and C_s. It is also worth noting that when the parameters k_{32}, k_{42}, k_{52} and k_{62} are all set equal to zero, the concentration C_{sb} (because of its initial condition that at $t = 0$, $C_{sb} = 0$) also becomes equal to zero for all times, and thus, kinetic model 1 (where $C_s = C_{sa}$) is obtained from kinetic model 2 under these conditions.

Finite bath with non-porous adsorbent particles

In the previous section porous adsorbents were considered, since it is common to use porous particles in order to obtain high macromolecule adsorption capacities per unit volume. But the porous adsorbent particles, for a given mode of operation, would have a higher overall mass transfer resistance (because of the intraparticle mass transfer resistance) than that encountered in non-porous adsorbent particles of the same dimension. In non-porous adsorbents the ligands are immobilized on the outer surface of the particle.

For single component adsorption in a finite bath with non-porous adsorbent particles, eqn. 1 assumes the following form:

$$\frac{dC_d}{dt} = \left(\frac{1-\varepsilon}{\varepsilon}\right)\left(\frac{\alpha+1}{r_0}\right) K_f(C_{dp} - C_d) \tag{14}$$

In eqn. 14, C_{dp} denotes the concentration of the adsorbate in the liquid layer adjacent to the surface of the non-porous adsorbent particle. Since $dC_d/dt = -[(1-\varepsilon)/\varepsilon](dC_s/dt)$, the term dC_s/dt would be given by eqn. 15

$$\frac{dC_s}{dt} = \left(\frac{\alpha+1}{r_0}\right) K_f(C_d - C_{dp}) \tag{15}$$

where C_{dp} is related to C_s, as is shown below. The initial conditions for eqns. 14 and 15 are given by eqns. 2 and 5, respectively. The only remaining step is an equation for C_{dp}.

It is apparent that in order to develop an expression for C_{dp}, one has to consider the controlling mechanisms of the adsorption process (of course, only at equilibrium the value of C_{dp} should be equal to the value of C_d). The following two cases may be considered:

(i) It is assumed that adsorption is controlled by film mass transfer, and therefore, C_{dp} is taken to be in equilibrium with the concentration of the adsorbate in the adsorbed phase, C_s, at every point on the surface of the adsorbent particle. If, for example, the equilibrium adsorption data of a given system are described by the Langmuir isotherm given in eqn. 10, then the expression for C_{dp} would have the following form:

$$C_{dp} = \frac{C_s}{K(C_T - C_s)} \tag{16}$$

For this example, the right-hand-side of eqn. 16 should replace C_{dp} in eqns. 14 and 15, and the resulting non-linear ordinary differential equations will have to be integrated simultaneously in order to obtain the variation of C_d and C_s with time. If the equilibrium isotherm of an adsorption system is given by an expression other (*e.g.*, eqns. 12 and 13 with $\partial C_{sa}/\partial t = \partial C_{sb}/\partial t = 0$) than that shown in eqn. 10, then the expression for C_{dp} would have a form other than that given in eqn. 16.

(ii) It is considered that adsorption is controlled by film mass transfer and by the dynamics of the interaction (adsorption step) mechanism between the adsorbate and the ligand. In this case, C_{dp} and C_s are not in equilibrium. If, for example, kinetic model 1 described by eqn. 9 is considered to represent the dynamics of the adsorption step for a given system, then the concentration C_{dp} would be given (by combining eqns. 9 and 15) by the following expression:

$$C_{dp} = \frac{(\gamma C_d + k_{21} C_s)}{[k_{11}(C_T - C_s) + \gamma]} \tag{17}$$

where

$$\gamma = \left(\frac{\alpha + 1}{r_0}\right) K_f \tag{18}$$

For this example, the right-hand-side of eqn. 17 should replace C_{dp} in eqns. 14 and 15, and the resulting non-linear ordinary differential equations will have to be integrated simultaneously in order to obtain the variation of C_d and C_s with time. If the rate of the adsorption step is described by an expression other (*e.g.*, eqns. 12 and 13 of kinetic model 2) than that of kinetic model 1, then the expression for C_{dp} would have a form other than that given in eqn. 17. In this study, all calculations involving non-porous adsorbent particles (finite bath and column systems) have been carried out by considering that adsorption is controlled by film mass transfer and by the dynamics of the adsorption step [*i.e.*, in this study case (ii) has been considered].

The value of the film mass transfer coefficient, K_f, of the adsorbate in eqns. 1, 6, 14, 15 and 18, was calculated from the following expression [23]:

$$K_f = \frac{2D_{mf}}{d_p} + 0.31\left[\frac{(\Delta\rho)\mu g}{\rho^2}\right]^{1/3}\left(\frac{\mu}{\rho D_{mf}}\right)^{-2/3} \tag{19}$$

where D_{mf} denotes the diffusion coefficient of the adsorbate in free solution; d_p is the mean diameter of the adsorbent particles; $\Delta\rho$ is the density difference between the particulate and continuous phases; ρ is the density of the liquid solution; μ is the viscosity; and $g = 9.80665$ m/s^2.

Column with porous adsorbent particles

Single-component adsorption is considered to take place from a flowing liquid stream in a fixed bed of particles under isothermal conditions, and the concentration gradient in the radial direction of the bed is considered to be not significant [4,13,16,24]. A differential mass balance for the adsorbate in the flowing fluid stream gives

$$\frac{\partial C_d}{\partial t} - D_L\frac{\partial^2 C_d}{\partial x^2} + \frac{V_f}{\varepsilon}\frac{\partial C_d}{\partial x} = \left(\frac{1-\varepsilon}{\varepsilon}\right)\left(\frac{\alpha+1}{r_0}\right)K_f[C_p(t,x,r_0) - C_d] \tag{20}$$

In eqn. 20 the velocity of the fluid stream, V_f, is taken to be independent of the space variable x, because the liquid solutions encountered in affinity chromatography systems are very dilute and the main component of the solution is the carrier fluid (for non-dilute solutions a material balance, as shown in ref. 25, would provide the expression for $\partial V_f/\partial x$). The pressure drop through the fixed bed can be determined by the methods reported in pp. 129–134 of the book by Geankoplis [23]. The initial and boundary conditions of eqn. 20 are as follows:

$$C_d = 0 \qquad \text{at} \qquad t = 0, \qquad 0 \leqslant x \leqslant L \tag{21}$$

$$\frac{V_f}{\varepsilon}C_d - D_L\frac{\partial C_d}{\partial x} = \frac{V_f}{\varepsilon}C_{d,in} \qquad \text{at} \qquad x = 0, \qquad t > 0 \tag{22}$$

$$\frac{\partial C_d}{\partial x} = 0 \qquad \text{at} \qquad x = L, \qquad t > 0 \tag{23}$$

The value of D_L may be estimated by the methods reported in ref. 26. In certain systems the axial dispersion coefficient, D_L, is so low that by setting its value equal to zero the error introduced in the prediction of the behavior of an affinity adsorption system is not significant [24,26]. When D_L is set equal to zero, the term $D_L(\partial^2 C_d/\partial x^2)$, in eqn. 20, becomes equal to zero, and the boundary condition at $x = 0$ (eqn. 22) becomes as follows:

$$C_d = C_{d,in} \qquad \text{at} \qquad x = 0, \qquad t > 0 \tag{24}$$

The intraparticle diffusion mechanism of the adsorbate and the interaction mechanism between the adsorbate and the ligand for an affinity adsorption system in a column, should be the same as those in a finite bath (these are intrinsic mechanisms, as discussed earlier). For a given kinetic model of the adsorption mechanism (*e.g.*, kinetic model 1 or kinetic model 2) that would provide a satisfactory expression for the term $\partial C_s/\partial t$ in eqn. 3, the resulting equation for $\partial C_s/\partial t$ and eqns. 3 and 20 will have to be solved simultaneously in order to obtain the variation of C_d, C_p and C_s with time and space.

Column with non-porous adsorbent particles

For single-component adsorption in a column with non-porous adsorbent particles, C_{dp} replaces $C_p(t,x,r_0)$ in eqn. 20 and the resulting expression is solved together [13] with eqn. 25

$$\frac{\partial C_s}{\partial t} = \left(\frac{\alpha + 1}{r_0}\right) K_f(C_d - C_{dp}) \tag{25}$$

The initial condition of eqn. 25 is as follows:

$$C_s = 0 \qquad \text{at} \qquad t = 0, \qquad 0 \leqslant x \leqslant L \tag{25a}$$

The solution of these equations provides the variation of C_d and C_s with time and space. In this study, an expression for C_{dp} developed under the conditions of case (ii) discussed above, was employed in eqns. 20 and 25.

The value of the film mass transfer coefficient, K_f, of the adsorbate in the column (eqns. 3, 6, 20 and 25) was calculated from the expression given in eqn. 5 of ref. 13. For the column systems studied in this work, the estimated values of D_L were so low that D_L was set equal to zero in eqns. 20 and 22. By setting D_L equal to zero, the error introduced in the calculated dynamic behavior of the column systems was insignificant.

Computational methods

The method of orthognal collocation [27,28] was applied to the space variable r of the partial differential equation that describes mass transfer in the porous adsorbent particles, while the method of characteristics [28] was applied to the partial differential equation that describes mass transfer in the flowing fluid stream of the column ($D_L = 0$). The ordinary differential equations of the systems having porous adsorbent particles, were numerically integrated by using a third-order semi-implicit Runge–Kutta method (see ref. 28) developed by Michelsen [29]. The ordinary differential equations of the systems having non-porous adsorbent particles, were solved numerically by Gear's method (see ref. 28). The value of the effective pore diffusivity, D_p, as well as the values of the rate constants in kinetic models 1 and 2, were estimated by matching the equilibrium and dynamic (batch) experimental data with the theoretical predictions obtained from the solution of the equations of the models, through the use of a modified (non-linear least squares) Levenberg–Marquardt method (see ref. 30).

RESULTS AND DISCUSSION

The affinity chromatography systems studied in this work, involve (a) the adsorption of β-galactosidase onto monoclonal antibody ligand immobilized on porous silica particles [1], and (b) the adsorption of β-galactosidase onto monoclonal antibody ligand immobilized on non-porous glass coated beads [19,31]. Kinetic model 1 and kinetic model 2 are taken to represent two different dynamic mechanisms for the adsorption of β-galactosidase onto immobilized monoclonal antibody (anti-β-galactosidase) ligand. In our studies with kinetic model 2, spontaneous desorption of adsorbate from the complexes of "form a" and "form b" was not considered, and thus, k_{22} and k_{52} were set equal to zero. The desorption of adsorbate from the complexes of "form a" and "form b" was considered to occur only by macromolecule (β-galactosidase)-induced exchange interactions ($k_{42} \neq 0$, $k_{62} \neq 0$), and thus, the desorption mechanism of kinetic model 2 was made to be significantly different than that of kinetic model 1 (only spontaneous desorption is considered in kinetic model 1 with $k_{21} \neq 0$).

In Fig. 1, curve 1 represents the equilibrium data (equilibrium isotherm at $T = 293$ K) of the adsorption of β-galactosidase onto anti-β-galactosidase immobilized on porous silica particles [1]. The Langmuir (eqn. 10) expression with $C_T = 2.2$ mg/cm^3 and $K = 4.54 \cdot 10^3$ cm^3/mg, describes [1] curve 1. Curve 2 represents the best fit for the equilibrium data when kinetic model 2 with $\delta = 1$ and $\partial C_{sa}/\partial t = \partial C_{sb}/\partial t = 0$, is employed. The values of the parameters of the equilibrium expressions that describe curve 2 are as follows: $C_T = 2.2$ mg/cm^3; $K_1 = k_{12}/k_{32} = 2.0 \cdot 10^3$; $K_2 = k_{42}/k_{32} = 32.2$; $K_3 = k_{62}/k_{32} = 3.55 \cdot 10^3$; and $k_{22} = k_{52} = 0$. It is worth noting that although curves 1 and 2 are described by significantly different equilibrium adsorption models, the quantitative differences between the two curves are not large. In fact, the quantitative differences are rather very small for all values of the concentration of β-galactosidase greater than $2 \cdot 10^{-4}$ mg/cm^3. The data in curve 3 of Fig. 1 have been obtained from the same equilibrium expressions that describe curve 2 (the values of C_T, K_1, K_2, K_3, k_{22} and k_{52} in curve 3, are the same as those used in curve 2), but in curve 3 the value of δ is equal to 2. The quantitative differences between curves 2 and 3 are very small for intermediate and high adsorbate concentrations. At very low concentrations of β-galactosidase, the quantitative differences between curves 2 and 3 are larger (the largest difference of about 20.76% occurs at $C_d = 10^{-4}$ mg/cm^3) because at these low C_d values the concentration of the adsorbate in the complex of "form b", C_{sb}, is not insignificant, and thus, $\delta C_{sb} = 2C_{sb}$ (curve 3) is greater than $\delta C_{sb} = 1C_{sb}$ (curve 2), in eqns. 12 and 13. This may explain why the adsorptivity described by curve 2 is higher than that described by curve 3. It should be noted at this point that the agreement between curves 1 and 2 is better than that between curves 1 and 3. For this reason, the value of δ was taken to be equal to one in all subsequent model calculations (Figs. 2–5 and 7–10).

In Fig. 1, curve 4 represents the equilibrium data [19,31] (equilibrium isotherm at $T = 293$ K) of the adsorption of β-galactosidase onto anti-β-galactosidase immobilized on non-porous glass coated beads. The Langmuir equation with $C_T = 0.33490$ mg/cm^3 and $K = 19.120$ cm^3/mg, describes [19] curve 4. By comparing the values of the parameters (C_T and K) of the equations that describe curves 1 and 4, it is observed that the values of C_T and of the association constant, K, of the adsorption of

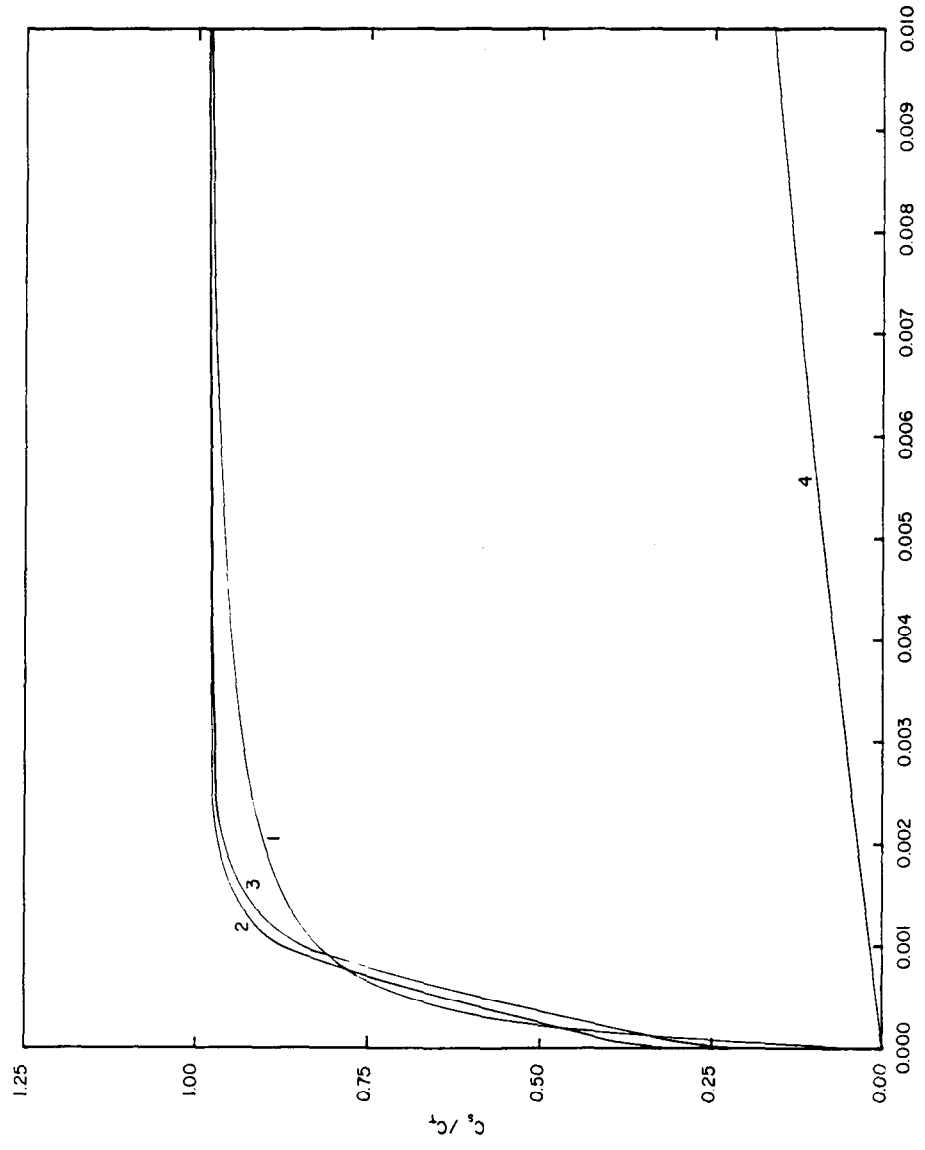

Fig. 1. Equilibrium adsorption isotherms; curves 1, 2 and 3 represent the adsorption of β-galactosidase onto anti-β-galactosidase immobilized on porous silica particles; curve 4 represents the adsorption of β-galactosidase onto anti-β-galactosidase immobilized on non-porous glass coated beads; curves 1 and 4 are obtained from eqn. 10; curves 2 and 3 are obtained from eqns. 12 and 13 when $\partial C_{sa}/\partial t = \partial C_{sb}/\partial t = 0$, and with $\delta = 1$ and $\delta = 2$, respectively; $T = 293$ K.

β-galactosidase onto anti-β-galactosidase immobilized on non-porous glass coated beads, are lower than the values obtained when the monoclonal antibody is immobilized on porous silica particles and the adsorbate interacts with the immobilized anti-β-galactosidase. The difference in the values of C_T may merely reflect differences in the total amounts of anti-β-galactosidase that can be coupled to the two different supports (porous silica particles; non-porous glass coated beads) which have different available surface areas per unit volume of particle. However, the difference in K values may be evidence for various alterations (*e.g.*, conformational changes [14,16]) occurring in the anti-β-galactosidase structure, when the monoclonal antibody is immobilized on different supports. These alterations may effect the ability of anti-β-galactosidase to bind adsorbate to varying extents. Chase [32] has also reported that in the equilibrium adsorption of β-galactosidase onto anti-β-galactosidase immobilized on porous silica particles and on Sepharose 4B, the values of C_T and K depended on which material the monoclonal antibody had been coupled to. The details of the experiments of the adsorption of β-galactosidase onto anti-β-galactosidase immobilized on non-porous glass coated beads as well as to the adsorption of β-galactosidase onto a control adsorbent, are reported in refs. 19 and 30. It is worth mentioning at this point that the equilibrium expressions obtained from kinetic model 2 (with $k_{22} = k_{52} = 0$) could not properly correlate the data represented by curve 4. Thus, kinetic model 2 was not employed in the dynamic calculations (finite bath and column systems) involving the adsorption of β-galactosidase onto anti-β-galactosidase immobilized on non-porous glass coated beads (Figs. 6 and 13–15).

In Fig. 2 the finite bath model predictions are compared with the experimental batch data of the adsorption of β-galactosidase onto monoclonal antibody ligand immobilized on porous silica particles. The dimensionless concentrations, C_d/C_{d0}, of the adsorbate in the fluid of the finite bath represented by curve 1, have been obtained from the batch model by employing kinetic model 1. The C_d/C_{d0} values of curve 2 have been obtained from the batch model when kinetic model 2 is employed. It is observed that the agreement between experiment and theory is satisfactory. Furthermore, the differences in the theoretical predictions of curves 1 and 2 are small although kinetic models 1 and 2 are different. It may also be observed that over the total operational time period, the agreement between curve 1 and the experimental data is slightly better than the agreement between curve 2 and the experimental data. The values of the rate constants that characterize the interaction mechanisms in kinetic models 1 and 2, were estimated by matching the predictions obtained from the expressions of the equilibrium (*i.e.*, eqn. 10, eqns. 12 and 13 with $\partial C_{sa}/\partial t = \partial C_{sb}/\partial t = 0$) and dynamic (batch) adsorption models with the corresponding equilibrium (equilibrium isotherm) and finite bath (dynamic) experimental data. The values of the mass transfer and interaction parameters for curves 1 and 2 are as follows:

Curve 1: $r_0 = 7.5 \cdot 10^{-3}$ cm, $\varepsilon = 0.985$, $\varepsilon_p = 0.5$, $K_f = 5.84 \cdot 10^{-4}$ cm/s, $D_p = 6.9 \cdot 10^{-8}$ cm^2/s, $k_{11} = 2.35 \cdot 10^{-2}$ cm^3/(mg)(s) and $k_{21} = 5.17 \cdot 10^{-6}$ s^{-1}.

Curve 2: $r_0 = 7.5 \cdot 10^{-3}$ cm, $\varepsilon = 0.985$, $\varepsilon_p = 0.5$, $K_f = 5.84 \cdot 10^{-4}$ cm/s, $D_p = 5.6 \cdot 10^{-8}$ cm^2/s, $k_{12} = 3.14 \cdot 10^{-2}$ cm^3/(mg)(s), $k_{22} = 0.0$, $k_{32} = 1.57 \cdot 10^{-5}$ cm^3/(mg)(s), $k_{42} = 5.06 \cdot 10^{-4}$ cm^3/(mg)(s), $k_{52} = 0.0$, $k_{62} = 5.58 \cdot 10^{-2}$ cm^3/(mg)(s) and $\delta = 1$.

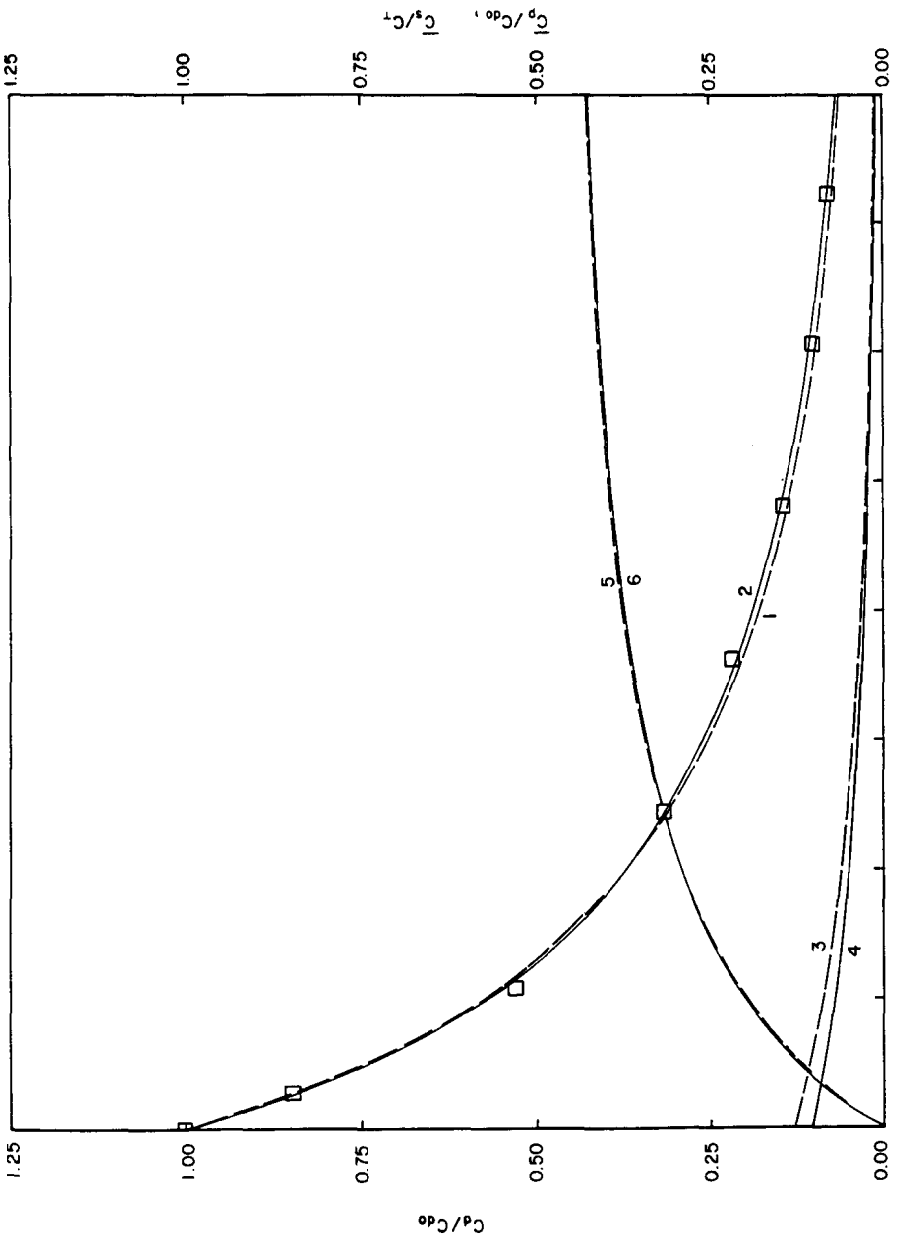

Fig. 2. Finite bath adsorption of β-galactosidase onto anti-β-galactosidase immobilized on porous silica particles; □ = experimental data; curves 1, 3 and 5 = predictions of the batch model employing kinetic model 1; curves 2, 4 and 6 = predictions of the batch model employing kinetic model 2 ($\delta = 1$). $C_{do} = 1.58 \cdot 10^{-2}$ mg/cm^3; $T = 293$ K.

The above data indicate that when kinetic model 2 is employed, the value of D_p, estimated by matching the experimental batch data with the predictions of the finite bath model, is smaller by 18.84% than that obtained when kinetic model 1 is used in the batch model. Furthermore, the value of the parameter k_{12} that characterizes the forward interaction rate for the formation of the complex of "form a" is about 33.62% larger than the value of k_{11}. The above comparisons may suggest that the finite bath model employing kinetic model 2 would provide a higher overall adsorption rate at earlier times (higher values of C_d) than that obtained from the finite bath using kinetic model 1, and the opposite would occur at longer times (lower values of C_d). This appears to be the case by comparing the predictions in curves 1 and 2. The value of the rate constant k_{32} suggests that the rate of formation of the complex of "form b" is very slow by comparison to the rate of formation of the complex of "form a" ($k_{12} \gg k_{32}$). In fact, the concentration C_{sb} is very much smaller than C_{sa}($C_{sa} \gg C_{sb}$) for most of the operational time, and furthermore, since k_{62} is about 110 times larger than k_{42} the desorption of adsorbate from the complex of "form b" is much faster than that from the complex of "form a". The values of the parameters k_{32} and k_{62} may suggest that a few adsorbed β-galactosidase molecules in "form a" change conformation to "form b", where the complex of "form b" may be considered to represent a complex which significantly facilitates the desorption of the adsorbed adsorbate by macromolecule-induced exchange interactions ($k_{62} \gg k_{42}$). Also, the parameter k_{21} that characterizes the desorption of adsorbed adsorbate in kinetic model 1, is much smaller than the value of k_{11}($k_{11} \gg k_{21}$). The above data and discussion could suggest that the reason for the very small differences between curves 1 and 2 (although the kinetic models 1 and 2 represent different overall adsorption mechanisms), is that the overall rate of adsorption of β-galatosidase onto anti-β-galactosidase immobilized on porous silica particles appears to be controlled by the forward interaction step of the overall adsorption mechanism (the forward interaction step is characterized by k_{11} in kinetic model 1, and by k_{12} in kinetic model 2) and by the intraparticle diffusion mechanism (characterized by D_p). Numerous simulations have shown that the effect of the film mass transfer resistance (characterized by K_f) on the overall rate of adsorption, is not as significant as the effects of pore diffusion and of the adsorption step. It was found that the variation of the estimated value ($K_f = 5.84 \cdot 10^{-4}$ cm/s) of K_f by $\pm 20\%$, has no significant effect on the dynamic behavior of the batch system. In Fig. 2, curves 3 and 4 represent the dynamic behavior of the dimensionless average concentration ($\bar{C}_p/C_{d0}$) of β-galactosidase in the pore fluid of the porous silica particles, obtained from the batch model by employing kinetic models 1 and 2, respectively. Curves 5 and 6 represent the dynamic behavior of the dimensionless average concentration of β-galactosidase in the adsorbed phase ($\bar{C}_s/C_T$) calculated from the finite bath model by using kinetic models 1 and 2, respectively (for kinetic model 2, $\bar{C}_s = \bar{C}_{sa} + \bar{C}_{sb}$). It can be observed that the differences between curves 3 and 4 are very small for most of the operational time. The differences between curves 3 and 4 are larger only at the very early times of the adsorption process, and would appear to have no effect (the use of kinetic model 1 or 2) on the overall dynamic performance of the adsorption process since the adsorption stage would be terminated at longer times where the differences between curves 3 and 4 are insignificant and a considerable amount of β-galactosidase would have been adsorbed. The differences between curves 5 and 6 are very small for all times of operation, and thus, the use of

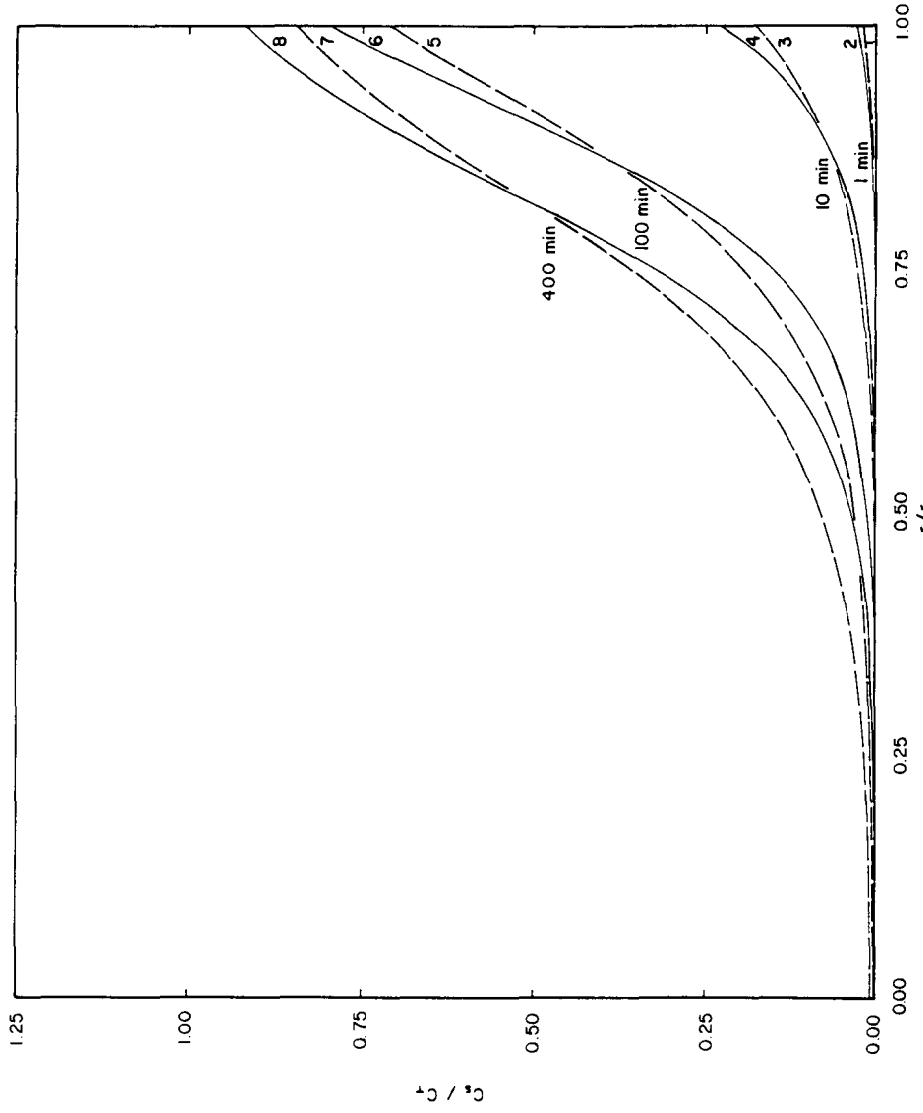

Fig. 3. Concentration profiles of β-galactosidase in the adsorbed phase of the porous adsorbent particles; curves 1, 3, 5 and 7 are obtained from the batch model employing kinetic model 1; curves 2, 4, 6 and 8 are obtained from the batch model employing kinetic model 2 ($\delta = 1$). Batch times: 1 min ≡ curves 1 and 2; 10 min ≡ curves 3 and 4; 100 min ≡ curves 5 and 6; 400 min ≡ curves 7 and 8. $C_{ao} = 1.58 \cdot 10^{-2}$ mg/cm^3; $T = 293$ K.

kinetic model 1 or 2 would appear to have no effect on the dynamic performance of the adsorption stage.

In Fig. 3, the dimensionless concentration profiles of adsorbed β-galactosidase in the adsorbent particle are presented at different times. The data obtained by using kinetic model 2 (curves 2, 4, 6 and 8, where $C_s = C_{sa} + C_{sb}$) indicate that the capacity of the immobilized ligands at the outer parts of the adsorbent particle has been used more effectively than in the case where kinetic model 1 is used, and the profiles of curves 2, 4, 6 and 8 are steeper than those represented by curves 1, 3, 5 and 7. This may be due to the fact that $k_{12} > k_{11}$. On the other hand, the data in curves 1, 3, 5 and 7 have been obtained from a model whose pore diffusivity has a higher value than that of the system in curves 2, 4, 6 and 8, and this leads to a faster penetration of β-galactosidase to the interior of the adsorbent particle and to the higher values of C_s/C_T in the interior parts of the particle for the system in curves 1, 3, 5 and 7. The differences in the adsorbed concentration profiles shown in Fig. 3, do not lead to any significant differences for the values of the average adsorbed concentrations ($\bar{C}_s/C_T$) in the adsorbent particles, as curves 5 and 6 of Fig. 2 indicate. This may occur because it appears that, in the adsorption of β-galactosidase onto anti-β-galactosidase immobilized on porous silica particles, the effect of restricted pore diffusion [12] is negligible and the phenomenon of percolation threshold [12] does not occur. The results may have been very different if an affinity chromatography system exhibiting restricted pore diffusion [12] had been considered, and it may be possible that in such a system kinetic model 2 may represent an adsorption mechanism which may be more appropriate than that of kinetic model 1, or the opposite may be the case (kinetic model 1 may be more appropriate than kinetic model 2).

But the results in Fig. 3 clearly show that different kinetic models (kinetic models 1 and 2) employed to describe the adsorption mechanism, can lead to significantly different concentration profiles for the adsorbate in the adsorbed phase; of course, they also lead to different concentration profiles for the adsorbate in the pore fluid (these concentration profiles in the pore fluid are not shown in Fig. 3). These differences in the concentration profiles within the adsorbent particles, may have important implications with regard to the operation of the wash and elution stages, since the wash and elution rates depend [1–4] on the concentration profiles of the adsorbate (in the pore fluid and adsorbed phase) that were established at the end of the adsorption stage. Thus, while the results in Fig. 2 indicate that kinetic models 1 and 2 do not lead to significant differences in the average concentrations of the adsorbate in the pore fluid and adsorbed phases of the adsorbent particles, the data in Fig. 3 strongly show that the two different kinetic models can lead to significant differences in the concentration profiles and this can have important implications [1–4] on the operation and performance of the wash and elution stages. This finding indicates that it is important in kinetic model discrimination studies [14,16,18] to identify the kinetic model that would provide an appropriate physical description of the adsorption mechanism of the finite bath model.

In Figs. 4 and 5, the effect of varying the estimated value of the pore diffusivity, D_p, by $\pm 20\%$ is examined. In Fig. 4 the finite bath model uses kinetic model 1, while in Fig. 5 kinetic model 2 is employed. It can be observed that, at the earlier times of the adsorption process, the differences between curves 1, 2 and 3 and between curves 4, 5 and 6, are not significant because at those earlier times the concentration gradient in

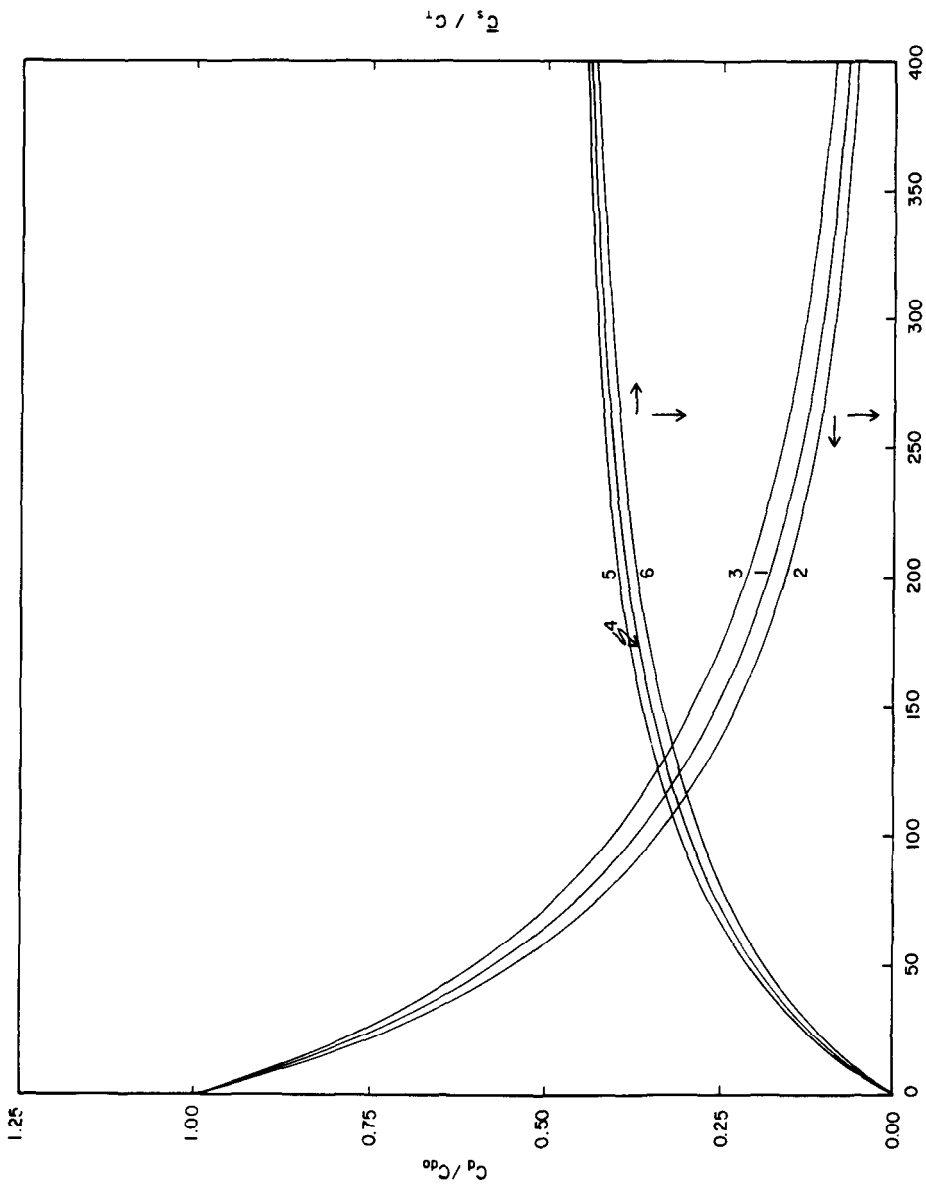

Fig. 4. The effect of the variation of the estimated value of D_p by $\pm 20\%$, on the dynamic behavior of C_d/C_{d0} and $\bar{C}_s/C_T$. The results are obtained from the batch model employing kinetic model 1. $D_p = 6.9 \cdot 10^{-8}$ cm^2/s in curves 1 and 4; $D_p = 1.2\,(6.9 \cdot 10^{-8})$ cm^2/s in curves 2 and 5; $D_p = 0.8\,(6.9 \cdot 10^{-8})$ cm^2/s in curves 3 and 6. $C_{d0} = 1.58 \cdot 10^{-2}$ mg/cm^3; $T = 293$ K.

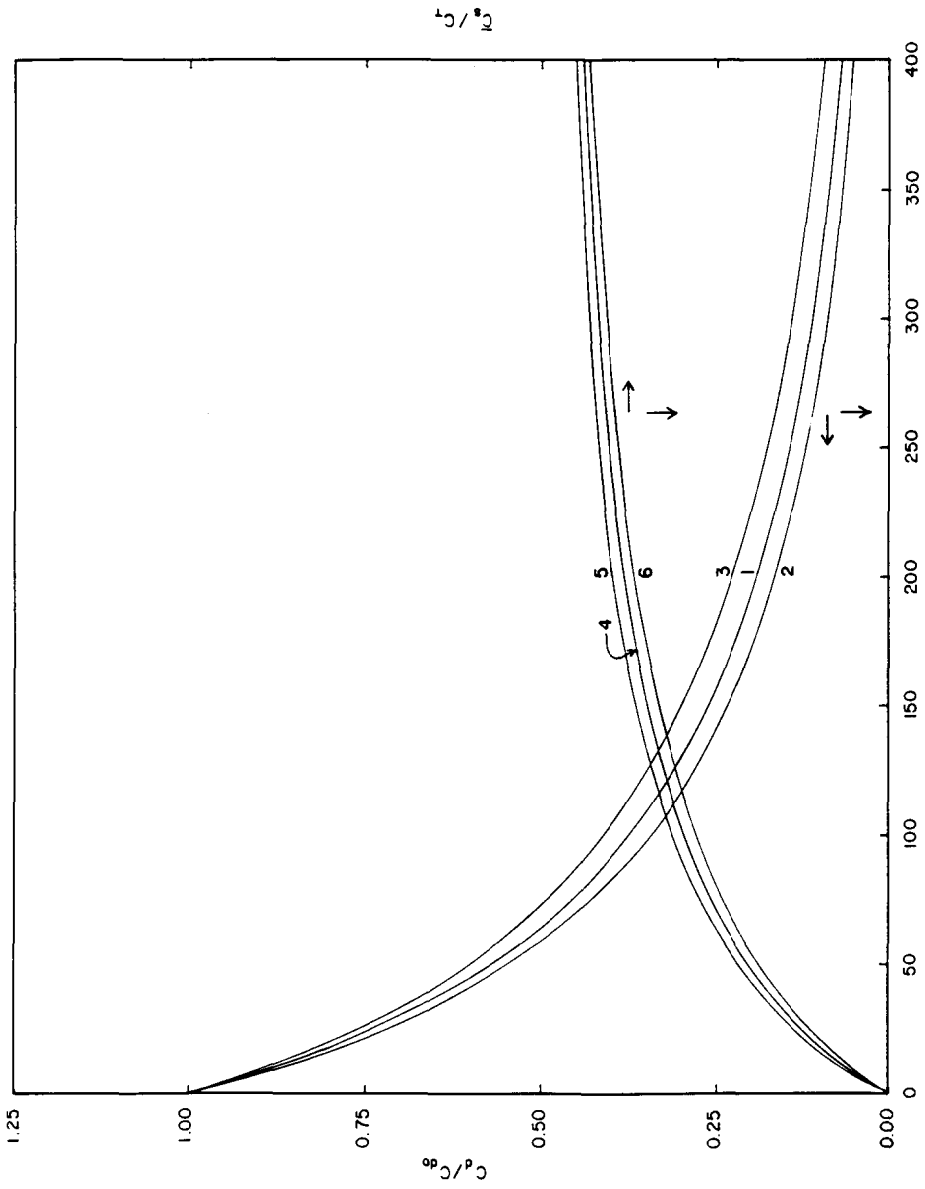

Fig. 5. The effect of the variation of the estimated value of D_p by $\pm 20\%$, on the dynamic behavior of C_d/C_{d0} and $\bar{C}_s/C_T$. The results are obtained from the batch model employing kinetic model 2 ($\delta = 1$). $D_p = 5.6 \cdot 10^{-8}$ cm^2/s in curves 1 and 4; $D_p = 1.2\,(5.6 \cdot 10^{-8})$ cm^2/s in curves 2 and 5; $D_p = 0.8\,(5.6 \cdot 10^{-8})$ cm^2/s in curves 3 and 6. $C_{d0} = 1.58 \cdot 10^{-2}$ mg/cm^3; $T = 293$ K.

the pore fluid ($\partial C_p/\partial r$) is high, and the mass transfer rate of the adsorbate in the porous particle is high and less sensitive to the value of D_p. At large times, the concentration gradient in the pore fluid is small and this leads to a significantly decreased mass transfer rate, which is slightly more sensitive (for the affinity chromatography system and the operational times presented in Figs. 4 and 5) to the value of D_p when compared with the effect at earlier times. The largest effect of D_p on C_d/C_{d0} and $\bar{C}_s/C_T$ occurs at intermediate times, where the concentration gradient, $\partial C_p/\partial r$, has moderate values and the sensitivity of the mass transfer rate on the value of D_p could increase significantly, as it can be observed for the sytems in Figs. 4 and 5. Also, while the change in the estimated value of D_p is symmetric ($\pm 20\%$) the effect of this change on C_d/C_{d0} and $\bar{C}_s/C_T$ is asymmetrical. Furthermore, it appears that the variation of the estimated value of D_p affects the dynamic behavior of C_d/C_{d0} more than the dynamic behavior of $\bar{C}_s/C_T$. For the system in Fig. 5 the effect of the variation of the value of D_p on C_d/C_{d0} and $\bar{C}_s/C_T$ appears to be larger than the corresponding effect on the system in Fig. 4; it should be noted that the concentration gradient in the pore fluid is higher when kinetic model 2 is used (also the concentration gradient in the adsorbed phase is higher when kinetic model 2 is used, at it can be observed in Fig. 3). The above discussion and results in Figs. 4 and 5 suggest that (i) it is important to have an accurate value for the pore diffusivity, and (ii) if the value of D_p is estimated by matching the experimental finite bath data with the predictions of the batch model, it is important to use a proper kinetic model for the adsorption mechanism and emphasize in the estimation procedure the importance of the experimental data obtained at times after the initial adsorption rate period (the data at intermediate operational times).

In Fig. 6 the experimental batch data of the adsorption of β-galactosidase onto anti-β-galactosidase immobilized on non-porous glass coated beads, are presented. The results in curve 1 represent the theoretical predictions of the finite bath model when kinetic model 1 is taken to represent the adsorption mechanism. The agreement between the experimental results and curve 1 is considered to be reasonable. The parameters k_{11} and k_{21} were estimated by matching the predictions of the batch model with the experimental data. The values of the parameters of the batch model that provides the results of curve 1, are as follows: $\varepsilon = 0.895$, $r_0 = 0.86 \cdot 10^{-2}$ cm, $K_f = 2.64 \cdot 10^{-4}$ cm/s, $k_{11} = 6.19 \cdot 10^{-2}$ cm^3/(mg)(s), and $k_{21} = 0.32 \cdot 10^{-2}$ s^{-1}. The experimental methods and procedures used to obtain the experimental data in Fig. 6, are reported in refs. 19 and 31. Curve 2 describes the variation of the dimensionless concentration C_s/C_T with time. The effect of changing the estimated value ($K_f = 2.64 \cdot 10^{-4}$ cm/s) of K_f by $\pm 20\%$, has negligible effect on the dynamic behavior of C_d/C_{d0} and C_s/C_T for all operational times. The results in Fig. 6 suggest that if an appropriate estimate of the value of K_f can be obtained [1,18], then the dynamics of the kinetic model developed to represent the adsorption mechanism would play the most significant role in determining the adsorption rate in batch systems involving non-porous adsorbent particles. It is worth noting again that kinetic model 2 was not used to describe the adsorption mechanism of the affinity chromatography system in Fig. 6, because of the reason reported in the discussion of curve 4 of Fig. 1.

In Fig. 7 the breakthrough curves of the adsorption of β-galactosidase onto anti-β-galactosidase immobilized on porous silica particles, are presented for six different column lengths. Curves 1, 3, 5, 7, 9 and 11 represent the results obtained from the column model employing kinetic model 2 whose parameter values were taken to be

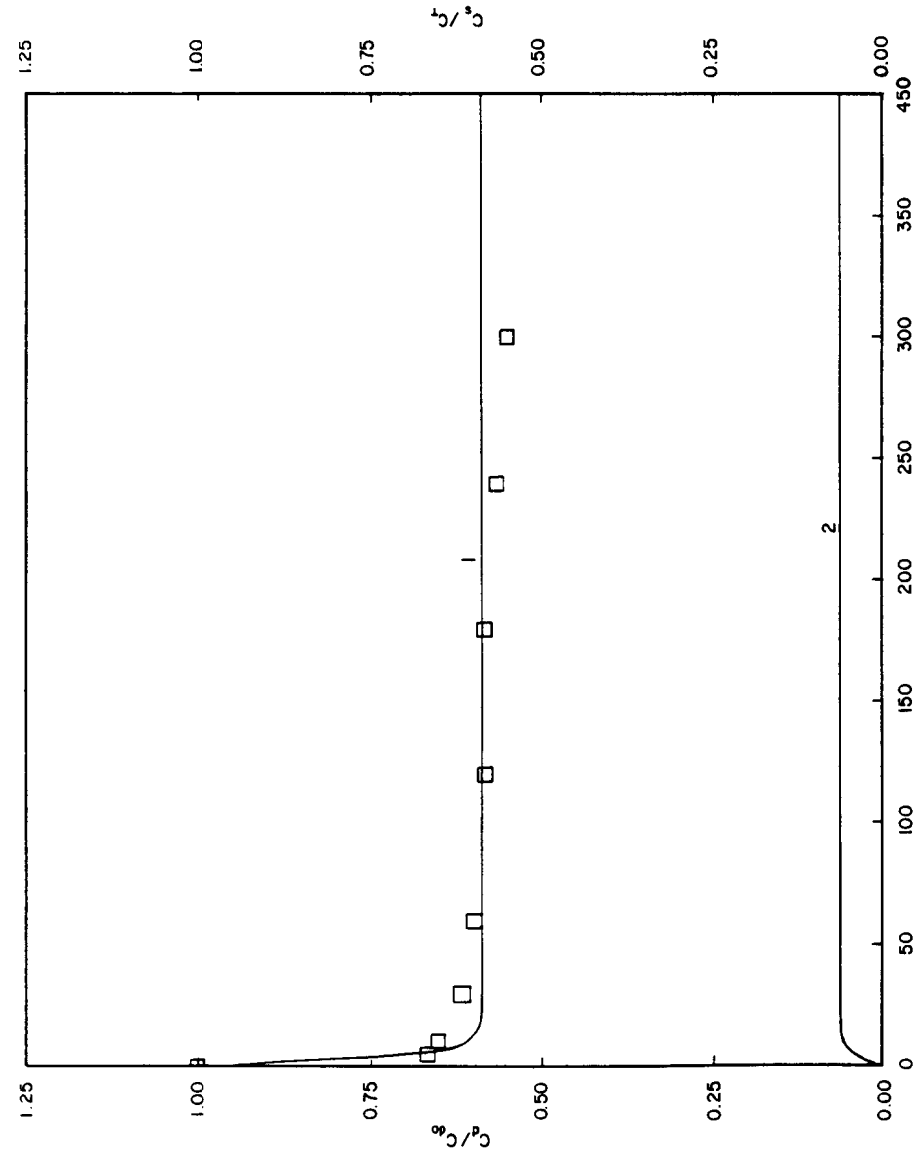

Fig. 6. Finite bath adsorption of β-galactosidase onto anti-β-galactosidase immobilized on non-porous glass coated beads; □ = experimental data; curves 1 (C_d/C_{d0} *versus* time) and 2 (C_s/C_T *versus* time) have been obtained from the batch model employing kinetic model 1; $C_{d0} = 6.0 \cdot 10^{-3}$ mg/cm^3; $T = 293$ K. When the estimated value of K_f ($K_f = 2.64 \cdot 10^{-4}$ cm/s) is varied by $\pm 20\%$, the results of C_d/C_{d0} coincide with curve 1 and those of C_s/C_T coincide with curve 2.

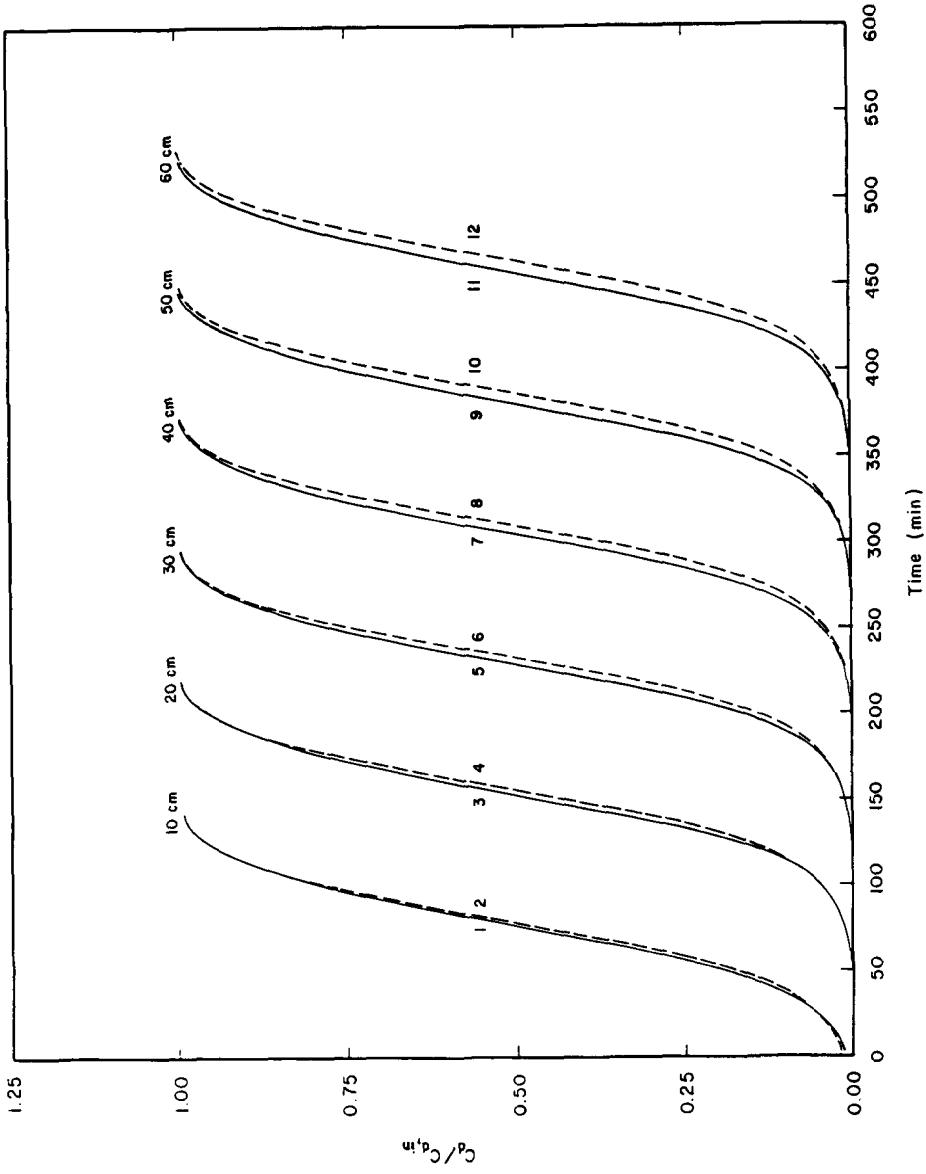

Fig. 7. Breakthrough curves of the adsorption of β-galactosidase onto anti-β-galactosidase immobilized on porous silica particles, for different column lengths; kinetic model 2 ($\delta = 1$) is used for curves 1, 3, 5, 7, 9 and 11; kinetic model 1 is used for curves 2, 4, 6, 8, 10 and 12. $C_{d,in} = 0.1$ mg/cm^3; $T = 293$ K.

the same as those estimated from the finite bath data; the value of the pore diffusivity was also taken to be the same as that estimated from the batch data, and thus, $D_p = 5.6 \cdot 10^{-8}$ cm^2/s. Curves 2, 4, 6, 8, 10 and 12 represent the results when kinetic model 1 is used to describe the adsorption mechanism in the column model, and the values of the rate constants k_{11} and k_{21} were taken to be the same as those estimated from the finite bath data; the value of the pore diffusivity was estimated from the batch data (curve 1 of Fig. 2) and its value is $D_p = 6.9 \cdot 10^{-8}$ cm^2/s. The values of other parameters used in the column model to obtain the results in Figs. 7–12 are as follows: $C_{d,in} = 0.1$ mg/cm^3, $r_0 = 5 \cdot 10^{-3}$ cm, $\varepsilon = 0.4$, $V_f = 3 \cdot 10^{-2}$ cm/s, $\varepsilon_p = 0.5$, $K_f = 8.93 \cdot 10^{-4}$ cm/s. For each column length, the results in Fig. 7 indicate that kinetic models 1 and 2 provide almost identical starting times of breakthrough. It is also observed that kinetic model 2 provides, for a given time, higher breakthrough values ($C_d/C_{d,in}$) than those obtained from kinetic model 1, except for the early phase of the breakthrough of the 10-cm column. The differences between the breakthrough curves obtained from the column model by employing kinetic models 1 and 2, increase as the column length increases. Furthermore, it is found that the largest difference, for a given column length, occurs in the neighborhood of 50% breakthrough. Of course, in practical operations it is most often the case that it is the earlier part of the breakthrough curve that is of most interest as the adsorption stage of an actual process would be terminated at less than 50% breakthrough. The results in Fig. 7 suggest that the performance of the adsorption stage can be influenced by the differences in the mechanisms of the kinetic models (kinetic models 1 and 2), and the differences in the mechanisms affect more the performance of longer columns. Furthermore, the effect on the performance of the adsorption stage will have implications on the operation and performance of the wash and elution stages [2,4]. The operation and performance of the wash and elution stages will also be influenced from the fact that the two kinetic models provide different concentration profiles (pore fluid and adsorbed phase) for the adsorbate in the adsorbent particles and along the length of the fixed bed, at the end of the adsorption stage. In Figs. 8 and 9 the concentration profiles of the adsorbate in the pore fluid and the adsorbed phase of the adsorbent particles, are presented at different positions along the column length and at the time of 10% breakthrough. Curves 1, 3, 5 and 7 in Figs. 8 and 9 have been obtained when kinetic model 1 is used in the column model, while curves 2, 4, 6 and 8 have been obtained by employing kinetic model 2. It can be observed that the concentration profiles obtained from kinetic models 1 and 2 are different for a given dimensionless axial position (x/L), and this could have significant implications [2,4] on the performance and operation of the elution and wash stages.

In Fig. 10 the time required to reach a certain level of breakthrough is plotted *versus* column length. It can be observed that lines 1, 3, 5 and 7 are essentially having the same slope; also lines 2, 4, 6 and 8 have essentially the same slope. The results in Figs. 7 and 10 suggest that constant-pattern behavior appears to occur for this adsorption system. In the initial region the mass transfer front spreads as it progresses, but some distance from the inlet it reaches an asymptotic form and after this asymptotic form has been estabished it progresses as a stable mass transfer zone with no further change in shape.

In Figs. 11 and 12 the effect on the breakthrough curve of the column having a length of 30 cm is presented when the estimated value of D_p is changed by $\pm 20\%$. It is observed that in the neighborhood of 50% breakthrough the effect is insignificant. The

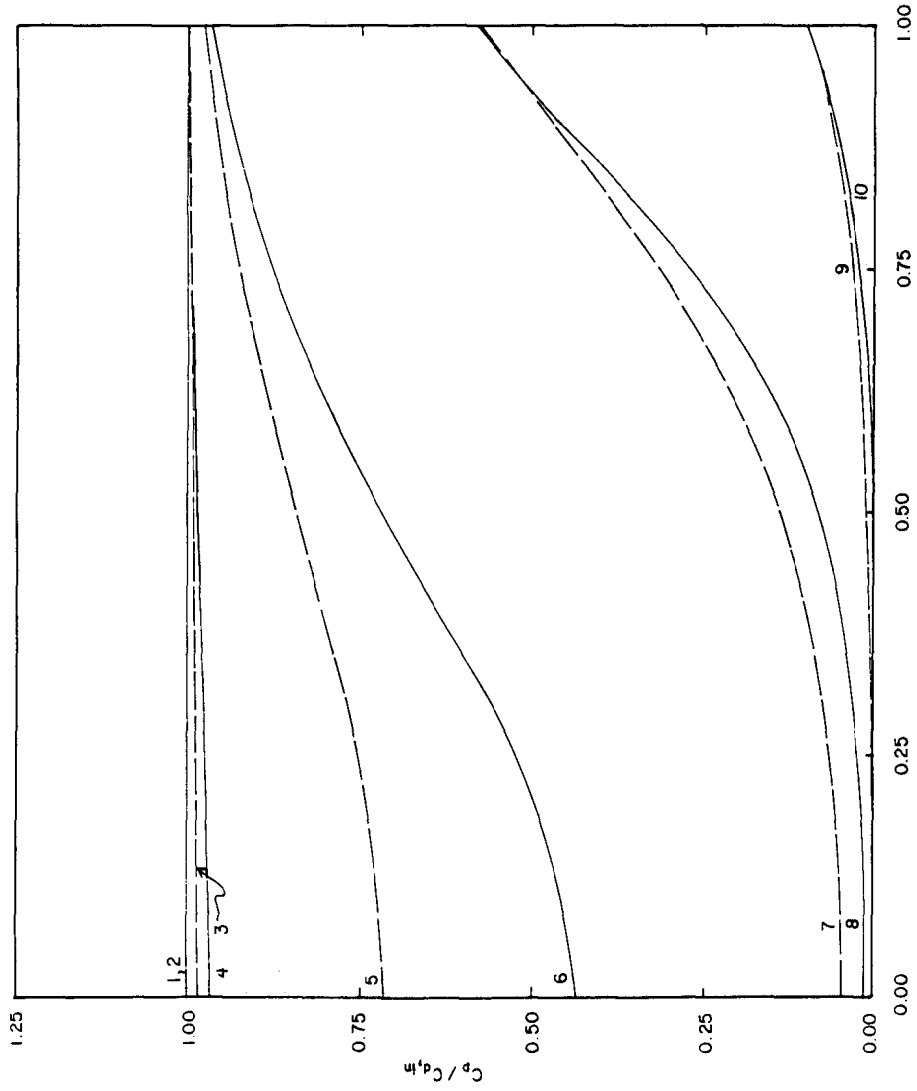

Fig. 8. Concentration profiles of β-galactosidase in the pore fluid of the adsorbent particles, at different positions along the length of a column of 30 cm; kinetic model 1 is used for curves 1, 3, 5, 7 and 9; kinetic model 2 ($\delta = 1$) is used for curves 2, 4, 6, 8 and 10. Dimensionless axial positions, x/L: 0.0 ≡ curves 1 and 2; 0.5 ≡ curves 3 and 4; 0.6 ≡ curves 5 and 6; 0.8 ≡ curves 7 and 8; 1.0 ≡ curves 9 and 10. $C_{d,in} = 0.1$ mg/cm^3; $T = 293$ K.

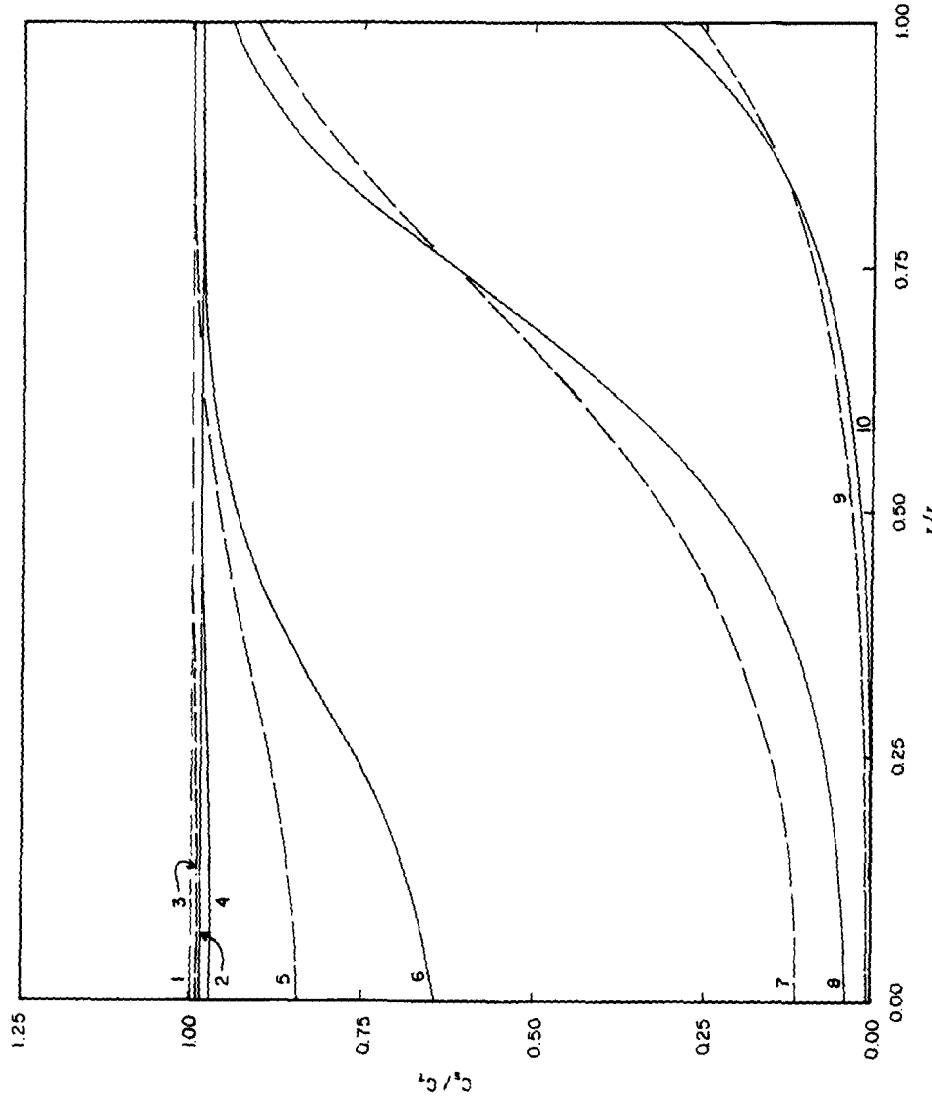

Fig. 9. Concentration profiles of β-galactosidase in the adsorbed phase of the adsorbent particles, at different positions along the length of a column of 30 cm; kinetic model 1 is used for curves 1, 3, 5, 7 and 9; kinetic model 2 ($\delta = 1$) is used for curves 2, 4, 6, 8 and 10. Dimensionless axial positions, x/L: 0.0 ≡ curves 1 and 2; 0.5 ≡ curves 3 and 4; 0.6 ≡ curves 5 and 6; 0.8 ≡ curves 7 and 8; 1.0 ≡ curves 9 and 10. $C_{s,in} = 0.1$ mg/cm^3; $T \approx 293$ K.

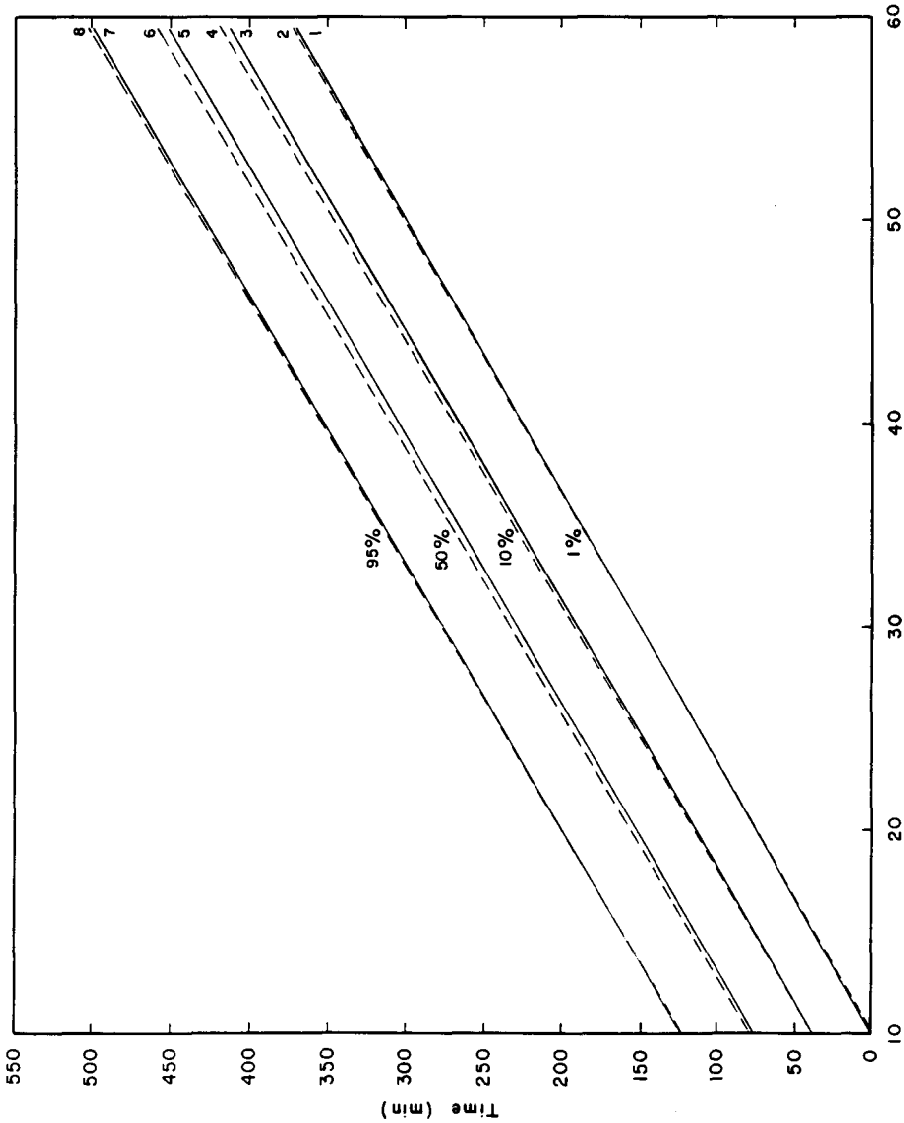

Fig. 10. Time required to reach a certain percentage of breakthrough for a given column length, in the adsorption of β-galactosidase onto anti-β-galactosidase immobilized on porous silica particles; kinetic model 2 ($\delta = 1$) is used for lines 1, 3, 5 and 7; kinetic model 1 is used for lines 2, 4, 6 and 8. $C_{d,in} = 0.1$ mg/cm^3; $T = 293$ K.

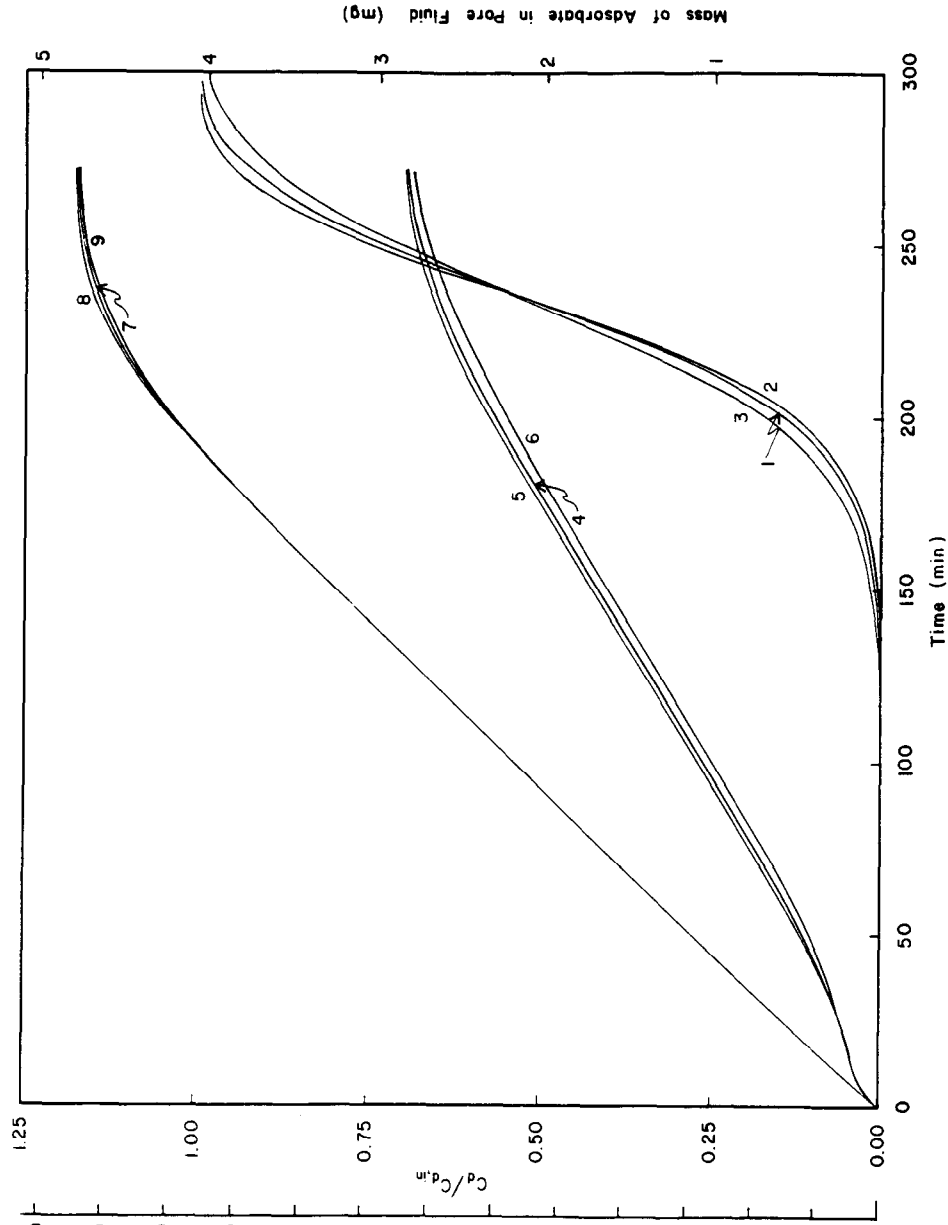

Fig. 11. The effect of the variation of the estimated value of D_p by $\pm 20\%$, on the dynamic behavior of $C_d/C_{d,in}$ and on the dynamic behavior of the mass of β-galactosidase in the pore fluid and adsorbed phases of the adsorbent particles, in a column of 30 cm; kinetic model 1 is used; curves 1, 2, 3 are for $C_d/C_{d,in}$; curves 4, 5, 6 are for the mass in the pore fluid; curves 7, 8, 9 are for the mass in the adsorbed phase; $D_p = 6.9 \cdot 10^{-8}$ cm^2/s in curves 1, 4 and 7; $D_p = 1.2\,(6.9 \cdot 10^{-8})$ cm^2/s in curves 2, 5 and 8; $D_p = 0.8\,(6.9 \cdot 10^{-8})$ cm^2/s in curves 3, 6 and 9. $C_{d,in} = 0.1$ mg/cm^3; $T = 293$ K.

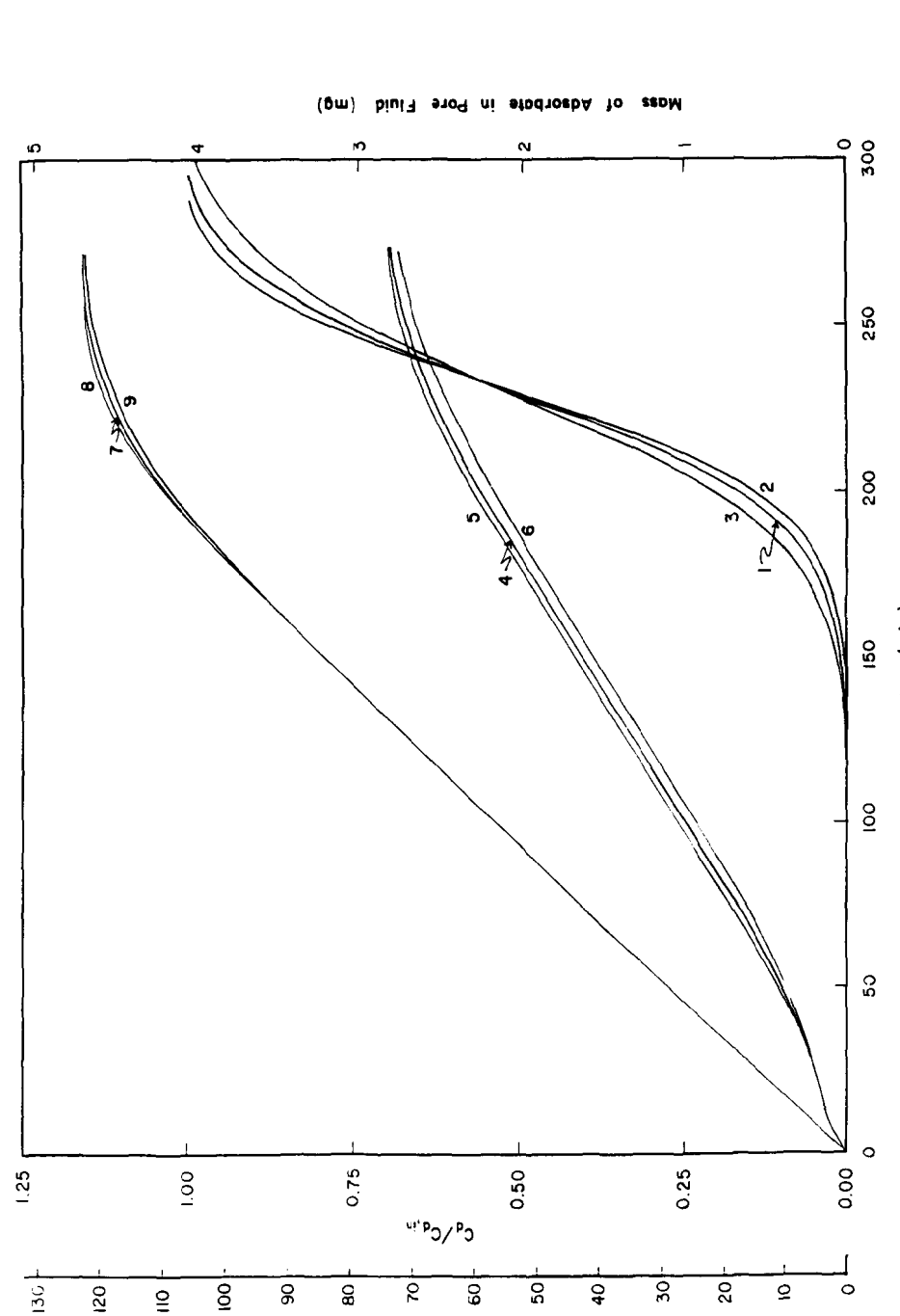

Fig. 12. The effect of the estimated value of D_p by $\pm 20\%$, on the dynamic behavior of $C_d/C_{d,in}$ and on the dynamic behavior of the mass of β-galactosidase in the pore fluid and adsorbed phases of the adsorbent particles, in a column of 30 cm; kinetic model 2 ($\delta = 1$) is used; curves 1, 2, 3 are for $C_d/C_{d,in}$; curves 4, 5, 6 are for the mass in the pore fluid; curves 7, 8, 9 are for the mass in the adsorbed phase; $D_p = 5.6 \cdot 10^{-8}$ cm^2/s in curves 1, 4 and 7; $D_p = 1.2$ ($5.6 \cdot 10^{-8}$) cm^2/s in curves 2, 5 and 8; $D_p = 0.8$ ($5.6 \cdot 10^{-8}$) cm^2/s in curves 3, 6 and 9. $C_{d,in} \approx 0.1$ mg/cm^3; $T = 293$ K.

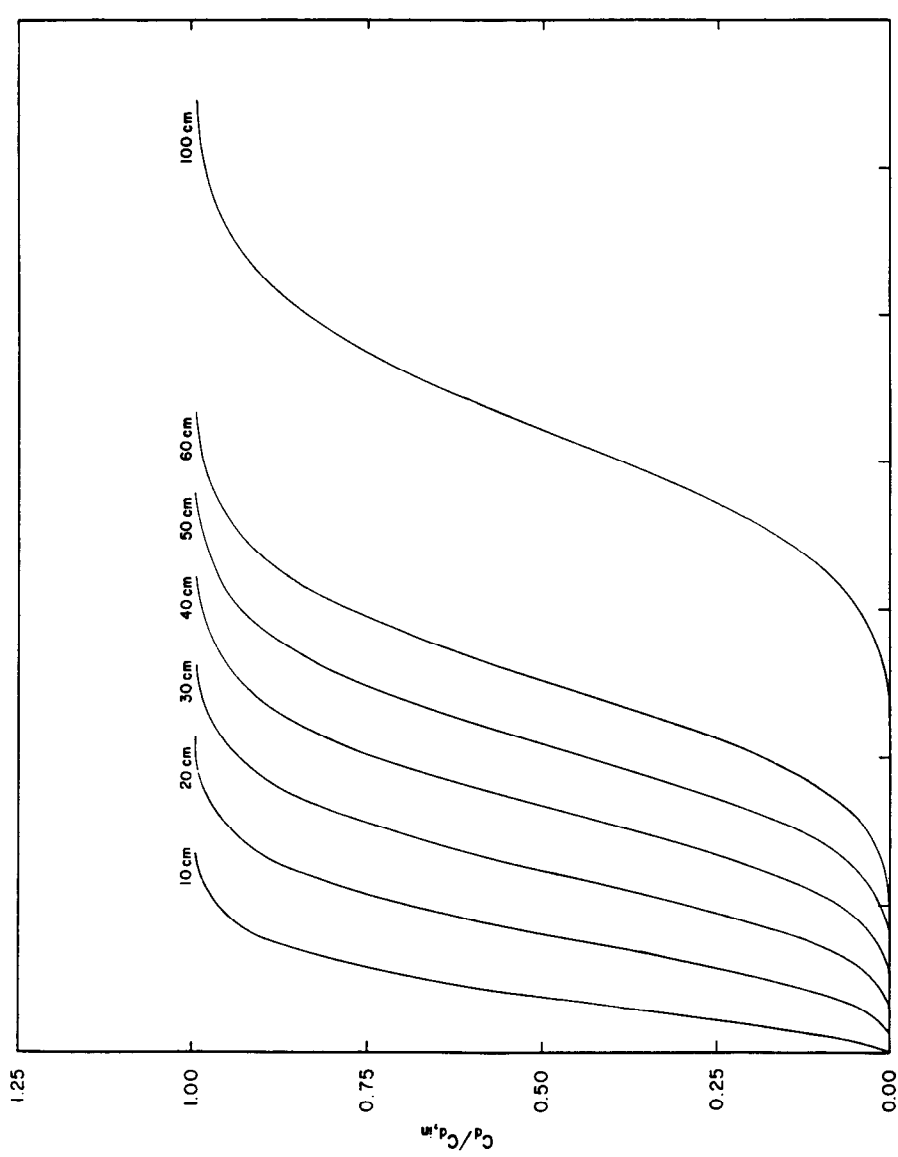

Fig. 13. Breakthrough curves of the adsorption of β-galactosidase onto anti-β-galactosidase immobilized on non-porous glass coated beads, for different column lengths. $C_{d,in} = 6.2 \cdot 10^{-3}$ mg/cm^3; $T = 293$ K.

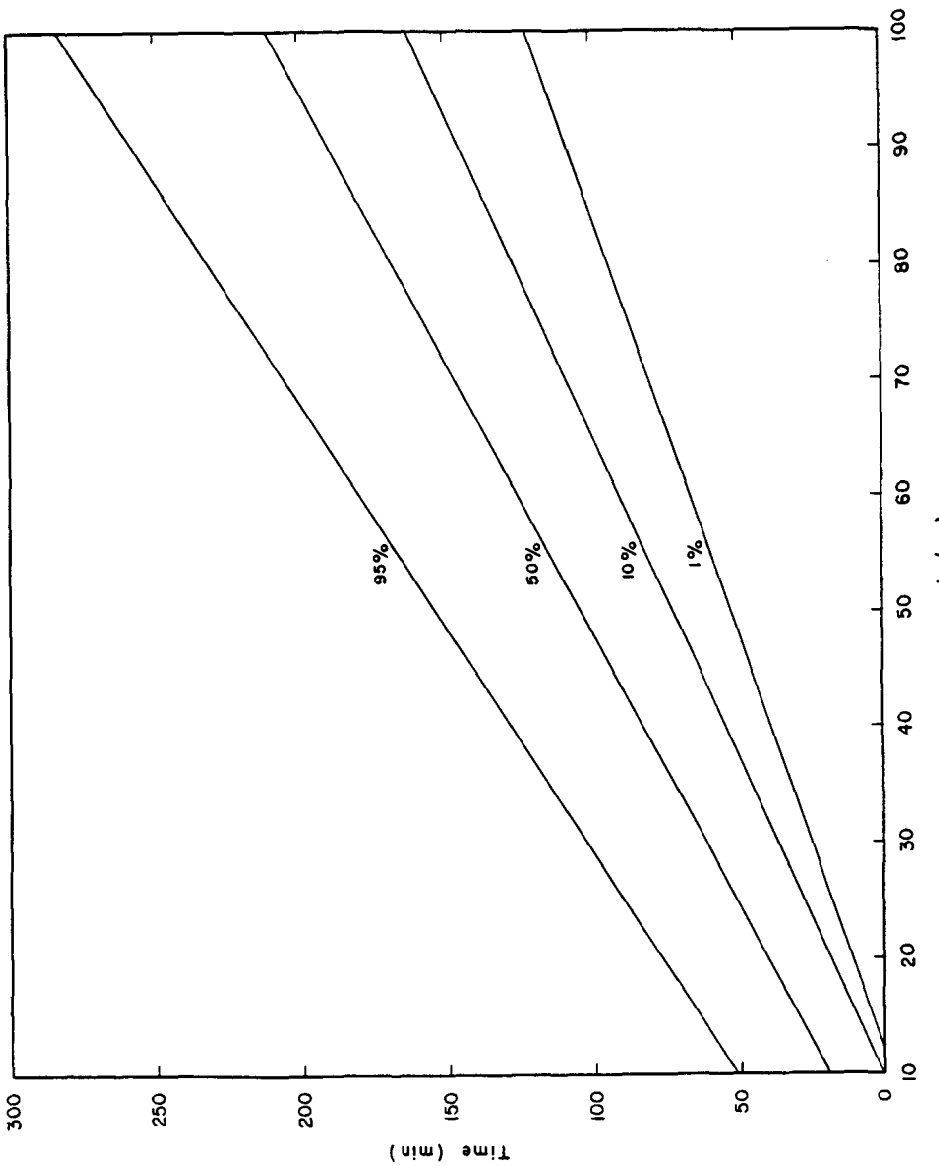

Fig. 14. Time required to reach a certain percentage of breakthrough for a given column length, in the adsorption of β-galactosidase onto anti-β-galactosidase immobilized on non-porous glass coated beads. $C_{d,in} = 6.2 \cdot 10^{-3}$ mg/cm^3; $T = 293$ K.

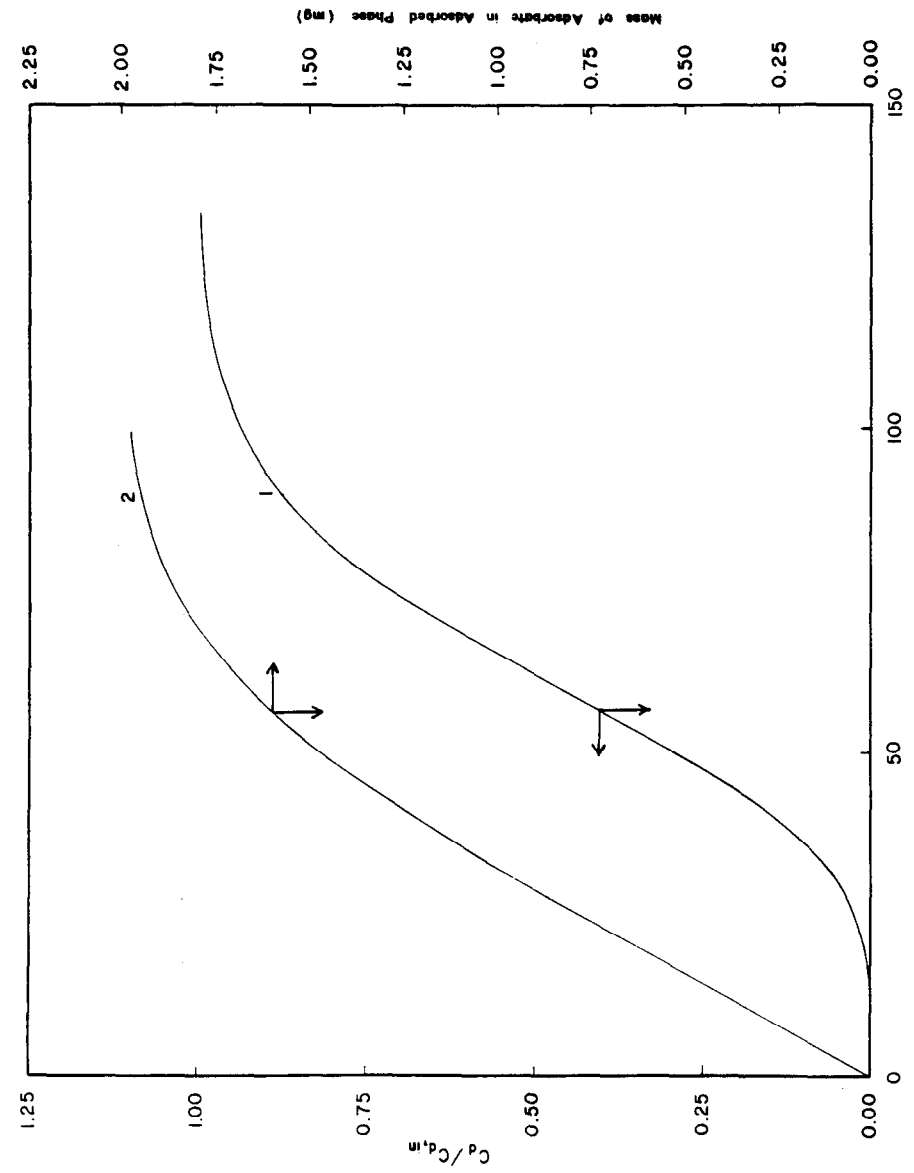

Fig. 15. The effect of the variation of the estimated value of K_f ($K_f = 4.38 \cdot 10^{-4}$ cm/s) by $\pm 20\%$, on the dynamic behavior of $C_d/C_{d,in}$ and on the dynamic behavior of the mass of β-galactosidase in the adsorbed phase of the non-porous adsorbent particles, in a column of 30 cm. The dynamic results obtained with $K_f = 1.2$ ($4.38 \cdot 10^{-4}$) cm/s, and with $K_f = 0.8$ ($4.38 \cdot 10^{-4}$) cm/s, coincide with the results obtained when $K_f = 4.38 \cdot 10^{-4}$ cm/s.

effect is also very small for the initial part and up to about 5% breakthrough. The effect increases after 5% breakthrough and starts decreasing again at about 25% breakthrough. These results suggest that if column switch occurs between 5% and 25% breakthrough, it is important to have an accurate value for D_p in order to predict properly the breakthrough curve, and thus, the column switch time. While the results in curves 7, 8 and 9 of Figs. 11 and 12 indicate that the effect of the variation of the estimated value of D_p on the total mass of adsorbed adsorbate is insignificant for most time after the start of breakthrough, the data in curves 4, 5 and 6 of Figs. 11 and 12 show that the variation of the value of D_p has a moderate effect on the total mass of the adsorbate in the pore fluid, and this effect could influence the operation and performance of the wash and elution [2,4] stages.

In Fig. 13 the theoretical breakthrough curves of the adsorption of β-galactosidase onto anti-β-galactosidase immobilized on non-porous glass coated beads, are presented for different column lengths. Kinetic model 1 was taken to represent the adsorption mechanism and the values of its parameters were the same as those used in the finite bath calculations with the non-porous adsorbent particles. The values of other parameters used in the column model that provided the results in Figs. 13–15, are as follows: $C_{d,in} = 6.2 \cdot 10^{-3}$ mg/cm^3, $\varepsilon = 0.4$, $V_f = 3 \cdot 10^{-2}$ cm/s, $r_0 = 0.86 \cdot 10^{-2}$ cm, and $K_f = 4.38 \cdot 10^{-4}$ cm/s. In Fig. 14 the times for different levels of breakthrough are plotted *versus* column length. The lines in Fig. 14 have different slopes, and this result is different than that obtained for the system in Fig. 10. The results in Figs. 13 and 14 indicate that the column length influences significantly the level of utilization [4] of the immobilized ligands, and this would have an effect on the performance of the wash and elution stages. In Fig. 15, the effect of the variation of the estimated value of K_f by $\pm 20\%$ is presented for a column of 30 cm. It is observed that the effect on the breakthrough curve and on the total amount of adsorbate in the adsorbed phase of the column, is insignificant; similar results were obtained for other column lengths.

CONCLUSIONS AND RECOMMENDATIONS

Finite bath and column models that could describe the adsorption of a single adsorbate onto ligand immobilized on porous or non-porous particles, were presented and solved.

Two different kinetic models were used to describe the dynamics of the adsorption mechanism (adsorption step) of the overall mass-transfer resistance of the adsorption of β-galactosidase onto monoclonal antibody immobilized on porous silica particles. The values of the ratios of certain parameters of the two kinetic models were estimated by matching the experimental equilibrium adsorption data with the predictions of the equilibrium expressions of the two kinetic models. The values of the remaining kinetic rate constants, as well as the value of the pore diffusivity, were estimated by matching the experimental batch (dynamic) data with the dynamic predictions of the finite bath model employing either kinetic model 1 or kinetic model 2. The agreement between the dynamic experimental data and the predictions of the finite bath model obtained by using kinetic model 1 or 2, was found to be satisfactory. The calculations show that the concentrations of the adsorbate in the fluid of the finite bath, as well as the average concentrations of the adsorbate in the pore fluid and in the adsorbed phase obtained from the batch model when kinetic

model 1 is employed, are not significantly different (quantitatively) than those obtained from the finite bath model when kinetic model 2 is used. But it was found that the two different kinetic models of the adsorption mechanism, lead to the estimation of different values for the pore diffusivity, D_p. These different values for the pore diffusivity, as well as the differences in the expressions describing the two different kinetic models of the adsorption mechanism, make the dynamic predictions of the concentration profiles of the adsorbate in the pore fluid and the adsorbed phase obtained by the batch model (or the column model) employing kinetic model 1, to be significantly different than those concentration profiles obtained when kinetic model 2 is used. The results in this study indicate that the two different kinetic models describe properly (quantitatively) the experimental overall mass-transfer resistance (the dynamic behavior of C_d/C_{d0} in the finite bath) of the batch adsorption system, but these two different kinetic models provide significantly different concentration profiles for the adsorbate in the pore fluid and adsorbed phases. These findings suggest that while proper (in quantitative terms) description of the experimental overall mass-transfer resistance may represent a necessary condition in model discrimination studies [14,16,18,21] for the determination of an appropriate kinetic model for the adsorption mechanism, this condition may not also be sufficient for proper kinetic model discrimination. The results suggest that the experimental concentration profiles of the adsorbate in the pore fluid and the adsorbed phase of the adsorbent particles would provide, if measured at different batch operational times, additional very useful information, so that proper discrimination studies between different kinetic models of the adsorption mechanism could be performed. The availability of the experimental concentration profiles in the adsorbent particles, would not only contribute in the determination of the appropriate physical kinetic mechanism, but it would also lead to better estimates for the value of the pore diffusivity and for the values of the rate constants of the kinetic model determined to represent the adsorption mechanism. In practice, it may be difficult to measure the concentration profiles of the adsorbate in the pore fluid, but one might develop an experimental technique to measure the concentration profiles of the adsorbate in the adsorbed phase. For example, it might be possible, in certain affinity adsorption systems, to label the adsorbate molecules. The adsorption process could be terminated at a certain operational time, and the adsorbent particles may be embedded in gelatin and sliced quickly (so that the adsorbed concentration profiles do not change appreciably) into very small (*e.g.*, 10 μm) sections using a microtome. Examination of the sections using an appropriate sensor might provide information with regard to the concentration profile of the adsorbate in the adsorbed phase. Experts in experimental analytical methods may perhaps devise different experimental techniques for measuring the concentration profiles of the adsorbate in the adsorbent particles. It should be noted at this point that even if only experimental informaton about the concentration profiles of the adsorbate in the adsorbed phase may be obtained, this information together with the experimental batch data of the adsorbate concentration in the fluid of the finite bath, could (i) significantly increase the information base for the construction of models describing the pore diffusion and interaction (adsorption) mechanisms, and (ii) could also increase the accuracy of the parameter estimation and model discrimination strategies, so that the proper kinetic model for the adsorption mechanism is determined, and accurate values for the pore diffusivity and the rate constants of the

adsorption mechanism may be estimated. The above approach could also be applicable to affinity adsorption systems exhibiting restricted [12] pore diffusion; of course, it should be noted that such systems would involve more complex parameter estimation and model discrimination studies.

The results obtained from the column simulations (with porous adsorbents) indicate that the differences in the breakthrough curves obtained from kinetic models 1 and 2, increase as the column length increases. Furthermore, for a given time, the concentration profiles in the pore fluid and the adsorbed phase obtained from kinetic models 1 and 2, are very different, and they also differ with the position along the axial distance. These column results suggest that experimental breakthrough curves obtained from relatively long columns, as well as measured concentration profiles within the adsorbent particles along the axial distance of relatively long columns, would provide additional very useful information for kinetic model discrimination and parameter estimation studies that would involve column (model) calculations. The kinetic model and parameter values determined from the column calculations, should be compared with those determined from the batch (finite bath) calculations involving the experimental batch data. It should be noted that parameter estimation and kinetic model discrimination studies involving column systems with porous adsorbent particles, may not be practical [1–4,14,16,18] because the column calculations are much more tedious, complex, and time consuming (with respect to computational time) than the batch calculations; furthermore, the column experiments are more difficult, time consuming, and expensive than the finite bath experiments. Thus, it is easier to determine the kinetic model of the adsorption mechanism and to estimate the value of D_p and the values of the kinetic rate constants from batch systems, as discussed above. But after the kinetic model has been determined, it should be used in the column model to predict the breakthrough curve for a relatively long column. The theoretical breakthrough curve should then be compared with the experimental breakthrough curve of the same relatively long column; also the theoretical concentration profiles in the adsorbent particles at different positions along the axial distance should be compared with the experimental, if available, concentration profiles. If the differences between the experimental and theoretical column data are not significant, this could indicate that a proper kinetic model for the adsorption mechanism and a proper value for D_p were determined from the studies involving the batch experimental data and batch model (it is assumed here that the non-intrinsic mass-transfer mechanisms in the finite bath and column systems, are described accurately by appropriate [1–4,13,16,18] expressions in the batch and column models). It should be noted that the batch and column experiments suggested above, they should preferably be carried out at different temperatures and with different initial (C_{d0}) and inlet ($C_{d,in}$) adsorbate concentrations.

In the affinity adsorption systems with the porous silica particles, the variation of the estimated value of the film mass-transfer coefficient K_f by $\pm 20\%$, has no significant effect on the dynamic behavior of the batch and column systems. The effect of the variation of the estimated value of the pore diffusivity D_p by $\pm 20\%$ on the dynamic behavior of the batch and column systems, can be appreciable. Furthermore, the variation of the estimated value of D_p affects the dynamic behavior of the concentration profiles of the adsorbate within the adsorbent particles. As we discussed above, different kinetic models of the adsorption mechanism also provide different

concentration profiles for the adsorbate within the adsorbent particles. Since the performance and operation of the wash and elution stages depend [1–4] significantly on the concentration profiles of the adsorbate (in the adsorbent particles) established at the end of the adsorption stage, it is very important to estimate accurately the value of the pore diffusivity and to determine a proper kinetic model for the adsorption mechanism of the affinity chromatography system under consideration. This could allow the accurate estimation of the performance of the adsorption stage, and could provide accurate initial conditions [1–4] for estimating the performance of the wash and elution stages.

The adsorption of β-galactosidase onto anti-β-galactosidase immobilized on non-porous glass coated beads, was described by kinetic model 1. It was found that when the adsorption rate is considered to be controlled by film mass-transfer and the interaction mechanism (kinetic model 1), a reasonable agreement between the experimental batch data and the predictions of the batch model is obtained. The variation of the estimated value of the film mass-transfer coefficient by $\pm 20\%$, has no significant effect on the dynamic behavior of the batch and column systems. Thus, if an accurate estimate of the film mass-transfer coefficient can be obtained from an appropriate correlation [1–4,13,16,18,23] (for batch or column operation) then the kinetic model that describes the adsorption mechanism could be determined from parameter estimation and model discrimination studies involving experimental batch data and the predictions of the batch model. For these affinity adsorption systems (systems having non-porous adsorbent particles), the calculations involving the column model are not much more complex and time consuming than the finite bath calculations (this is not the case for the systems having porous adsorbent particles), and thus, the kinetic model of the adsorption mechanism could also be determined from parameter estimation and model discrimination studies involving the predictions of the column model and the experimental breakthrough curves obtained from (i) different inlet concentrations of the adsorbate, (ii) different column lengths, and (iii) different temperatures of operation.

NOTATION

A_1	molecule of adsorbate
A_a	area occupied by adsorbed molecule in "form a"
A_b	area occupied by adsorbed molecule in "form b"
A_1L_1	non-covalent adsorbate-ligand complex
C_d	concentration of adsorbate in the bulk fluid phase (finite bath), or in the flowing fluid stream (column), mg/cm^3
$C_{d,in}$	concentration of adsorbate at $x < 0$ when $D_L \neq 0$, or at $x = 0$ when $D_L = 0$, mg/cm^3
C_{d0}	initial concentration of adsorbate in bulk fluid phase of finite bath, mg/cm^3
C_{dp}	concentration of adsorbate in the liquid layer adjacent to the surface of a non-porous adsorbent particle, mg/cm^3
C_p	concentration of adsorbate in pore fluid, mg/cm^3
$\bar{C}_p$	average concentration of adsorbate in pore fluid, mg/cm^3
C_s	concentration of adsorbate in adsorbed phase, mg/cm^3
$\bar{C}_s$	average concentration of adsorbate in adsorbed phase, mg/cm^3

C_{sa} concentration of adsorbed adsorbate in "form a", mg/cm^3
C_{sb} concentration of adsorbed adsorbate in "form b", mg/cm^3
$\bar{C}_{sa}$ average concentration of adsorbed adsorbate in "form a", mg/cm^3
$\bar{C}_{sb}$ average concentration of adsorbed adsorbate in "form b", mg/cm^3
C_T maximum concentration of adsorbate in adsorbed phase when all available (accessible) ligand is utilized, mg/cm^3
D_L axial dispersion coefficient of adsorbate, cm^2/s
D_p pore diffusion coefficient of adsorbate (in adsorbent particle), cm^2/s
K_f film mass transfer coefficient of adsorbate, cm/s
K k_{11}/k_{21}, cm^3/mg
K_1 k_{12}/k_{32}, dimensionless
K_2 k_{42}/k_{32}, dimensionless
K_3 k_{62}/k_{32}, dimensionless
k_{11} rate constant in eqn. 9, cm^3/(mg)(s)
k_{21} rate constant in eqn. 9, s^{-1}
k_{12} rate constant in eqn. 12, cm^3/(mg)(s)
k_{22} rate constant in eqn. 12, s^{-1}
k_{32} rate constant in eqns. 12 and 13, cm^3/(mg)(s)
k_{42} rate constant in eqn. 12, cm^3/(mg)(s)
k_{52} rate constant in eqn. 13, s^{-1}
k_{62} rate constant in eqn. 13, cm^3/(mg)(s)
L column length, cm
L_1 vacant immobilized ligand
r radial distance in adsorbent particle, cm
r_0 radius of adsorbent particle, cm
t time, s
T temperature, K
V_f superficial fluid velocity, cm/s
x axial distance, cm

Greek letters

α form factor; 0, 1 and 2 for slab, cylinder and sphere, respectively
γ given by eqn. 18
δ A_b/A_a
ε void fraction in finite bath, or column
ε_p void fraction in porous adsorbent particle

ACKNOWLEDGEMENTS

The authors gratefully acknowledge that this work was supported by the Monsanto Company and the NATO Scientific Affairs Division under Grant No. 0770/88.

REFERENCES

1 B. H. Arve and A. I. Liapis, *AIChE J.*, 33 (1987) 179.
2 B. H. Arve and A. I. Liapis, *Biotechnol. Bioeng.*, 30 (1987) 638.

3 B. H. Arve and A. I. Liapis, *Biotechnol. Bioeng.*, 31 (1988) 240.
4 B. H. Arve and A. I. Liapis, *Biotechnol. Bioeng.*, 32 (1988) 616.
5 W. Norde, *Adv. Colloid Interface Sci.*, 25 (1986) 267.
6 I. Lundstrom, B. Ivarsson, U. Jonsson and H. Elwing, in W. J. Feast and H. S. Munro (Editors), *Polymer Surfaces and Interfaces*, Wiley, New York, 1987, pp. 201–230.
7 A. A. Gorbunov, A. Ye. Lukyanov, V. A. Pasechnik and A. V. Vakhrushev, *J. Chromatogr.*, 365 (1986) 205.
8 J. Hubble, *Biotechnol. Bioeng.*, 30 (1987) 208.
9 A. E. Mark, P. D. Jeffrey and L. W. Nichol, *J. Theor. Biol.*, 131 (1988) 137.
10 E. N. Lightfoot, M. C. M. Cockrem, S. J. Gibbs and A. M. Athalye, in N. N. Li and H. Strathmann (Editors), *Separation Technology*, Engineering Foundation, New York, 1988, pp. 122–154.
11 R. J. Yon, *J. Chromatogr.*, 457 (1988) 13.
12 J. H. Petropoulos, A. I. Liapis, N. P. Kolliopoulos, J. K. Petrou and N. K. Kanellopoulos, *Bioseparation*, 1 (1990) 69.
13 A. I. Liapis, A. B. Anspach, M. E. Findley, J. Davies, M. T. W. Hearn and K. K. Unger, *Biotechnol. Bioeng.*, 34 (1989) 467.
14 A. I. Liapis, *J. Biotechnol.*, 11 (1989) 143.
15 A. I. Liapis, in N. N. Li and H. Strathmann (Editors), *Separation Technology*, Engineering Foundation, New York, 1988, pp. 420–487.
16 A. I. Liapis, in A. B. Mersmann and S. E. Scholl (Editors), *Fundamentals of Adsorption (Proceedings of the Third International Conference on Fundamentals of Adsorption, Sonthofen, May 7–12, 1989)*, Engineering Foundation, New York, 1990.
17 B. H. Arve and A. I. Liapis, in A. I. Liapis (Editor), *Fundamentals of Adsorption*, Engineering Foundation, New York, 1987, pp. 73–87.
18 A. I. Liapis, *Sep. Purif. Methods*, 19 (1990) 133.
19 M. A. McCoy, B. J. Hearn and A. I. Liapis, *Chem. Eng. Commun.*, (1991) in press.
20 A. Johnston and M. T. W. Hearn, *J. Chromatogr.*, 512 (1990) 101.
21 D. M. Bates and D. G. Watts, *Non-Linear Regression Analysis and Its Implications*, Wiley-Interscience, New York, 1988.
22 B. J. Horstmann and H. A. Chase, *Chem. Eng. Res. Des.*, 67 (1989) 243.
23 C. J. Geankoplis, *Transport Processes and Unit Operations*, Allyn and Bacon, Boston, MA, 1983.
24 F. H. Arnold, H. W. Blanch and C. R. Wilke, *Chem. Eng. J.*, 30 (1985) B9.
25 J. H. Harwell, A. I. Liapis, R. Litchfield and D. T. Hanson, *Chem. Eng. Sci.*, 35 (1980) 2287.
26 F. H. Arnold, H. W. Blanch and C. R. Wilke, *Chem. Eng. J.*, 30 (1985) B25.
27 J. Villadsen and M. L. Michelsen, *Solution of Differential Equation Models by Polynomial Approximation*, Prentice-Hall, Englewood Cliffs, NJ, 1978.
28 C. D. Holland and A. I. Liapis, *Computer Methods for Solving Dynamic Separation Problems*, McGraw-Hill, New York, 1983.
29 M. L. Michelsen, *AIChE J.*, 22 (1976) 594.
30 J. J. Moré, B. S. Garbow and K. E. Hillstrom, *User Guide for MINPACK-1, Report ANL-80-74*, Argonne National Labs., Argonne, IL, 1980.
31 B. J. Hearn, *M.S. Thesis*, Department of Chemical Engineering, University of Missouri-Rolla, Rolla, MO, 1989.
32 H. A. Chase, *J. Chromatogr.*, 297 (1984) 179.